STOCK LOCATION

2 DATE RECEIVED: YR 74 MO 03 DAY 15

12 SCREEN: ☐ OBTAIN BETTER COPY ☐ OBTAIN AUTHORITY ☐ REJECT ☐ OUT OF PRINT SOD ☐ ERRATA

17 ACCESSION NUMBER: N74 - 18399

3 RECEIPT TYPE & FORMAT: ☐ LOAN ☐ LAST COPY ☒ PC ☐ MF ☐ 35 MM ☐ 16 MM ☐ MAGNETIC TAPE ☐ CARDS ☐ OTHER (BOX 16)

13A ANNOUNCEMENT: VOL 74 ISSUE 12

13B FAS: ☐ YES ☐ NO

☒ GRA ☐ WGA ☐ UNLAWN

18 PAGES: 102

19 SHEETS

20 LOW LIMIT: PC MF

21 ☐ SUB-SCRIP-TION

4 STOCK RECEIVED FOR SALE: PC 6 MF

5 LOAN ETC.: DUE OUT RET

14 REPRODUCTION INSTRUCTIONS: BLOWBACK → MAKE MICROFICHE ☐ YES ☒ NO

PRINT ↓	NO	1 UP	2 UP
NO	1	4	7
1 UP	2	5	8
2 UP	3	6	9
MIX	SAME SIZE	ORDER STOCK FROM ↓	

15 PRESTOCK: PC DUE IN . PC PRINT ✓ PC SOURCE TO ORDER MF PRINT CODE M

22 PRICES: $ 8,00 ☐ U UNIT ☐ E PC + MN BOX 16 ☒ P PC → ☐ M MN → ☐ WI ☒ DEMAND

23 CATEGORY 24 DISTR CODE 25 INITIALS ACC DB A

11 NOT FULLY: ☐ LEGIBLE ☐ COLOR

6 TRANSACTION: ☐ NEW ITEM DUPE ↓ SUPER-SEDES ↓ ☐ PRIOR NUMBER ↓

7: NASA-CR-134548

26 FILL FROM: PAPER COPY ETC. SS ↓ MICRO-NEGA-TIVE XN

27 PUBLIC RELEAS-ABILITY C

8 REPORT NUMBERS (XREF) ☐ →

16 REMARKS: NASA

9 RELATED DOCUMENT ☐ →

10 CONTRACTING OFFICE-BILLING CODE: NASA - 100

28 FORM, PRICE, ETC.: 1211

29 ANN CODE

1 ARCHIVES

FORM NTIS-77 (REV. 1-73) USCOMM-DC 11954-P73

U.S. DEPARTMENT OF COMMERCE
NATIONAL TECHNICAL INFORMATION SERVICE

DOCUMENT TRAVELER

5/15

NASA CR-134548
ASRL TR 154-5

EXPERIMENTAL AND DATA ANALYSIS TECHNIQUES FOR DEDUCING COLLISION-INDUCED FORCES FROM PHOTOGRAPHIC HISTORIES OF ENGINE ROTOR FRAGMENT IMPACT/INTERACTION WITH A CONTAINMENT RING

Raffi P. Yeghiayan
John W. Leech
Emmett A. Witmer

Aeroelastic and Structures Research Laboratory
Department of Aeronautics and Astronautics
Massachusetts Institute of Technology
Cambridge, Massachusetts 02139

October 1973

Prepared for
AEROSPACE SAFETY RESEARCH AND DATA INSTITUTE
LEWIS RESEARCH CENTER
NATIONAL AERONAUTICS AND SPACE ADMINISTRATION
CLEVELAND, OHIO 44135

NASA Grant NGR 22-009-339

NASA CR-134548
ASRL TR 154-5

EXPERIMENTAL AND DATA ANALYSIS TECHNIQUES FOR DEDUCING COLLISION-INDUCED FORCES FROM PHOTOGRAPHIC HISTORIES OF ENGINE ROTOR FRAGMENT IMPACT/INTERACTION WITH A CONTAINMENT RING

Raffi P. Yeghiayan

John W. Leech

Emmett A. Witmer

AEROELASTIC AND STRUCTURES RESEARCH LABORATORY
DEPARTMENT OF AERONAUTICS AND ASTRONAUTICS

MASSACHUSETTS INSTITUTE OF TECHNOLOGY

CAMBRIDGE, MASSACHUSETTS 02139

October 1973

Prepared for

AEROSPACE SAFETY RESEARCH AND DATA INSTITUTE
LEWIS RESEARCH CENTER
NATIONAL AERONAUTICS AND SPACE ADMINISTRATION
CLEVELAND, OHIO 44135

NASA Grant NGR 22-009-339

I.

1. Report No. NASA CR-134548	2. Government Accession No.	3. Recipient's Catalog No.
4. Title and Subtitle Experimental and Data Analysis Techniques for Deducing Collision-Induced Forces from Photographic Histories of Engine Rotor Fragment Impact/Interaction with a Containment Ring		5. Report Date: October 1973 6. Performing Organization Code
7. Author(s) Raffi P. Yeghiayan, John W. Leech, and Emmett A. Witmer		8. Performing Organization Report No. ASRL TR 154-5 10. Work Unit No.
9. Performing Organization Name and Address Massachusetts Institute of Technology Aeroelastic and Structures Research Laboratory Cambridge, Massachusetts 02139		11. Contract or Grant No. NGR 22-009-339 13. Type of Report and Period Covered Contractor Report
12. Sponsoring Agency Name and Address National Aeronautics and Space Administration Washington, D.C. 20546		14 Sponsoring Agency Code

15. Supplementary Notes

Technical Monitors: Patrick T. Chiarito and Solomon Weiss, Aerospace Safety Research and Data Institute

Technical Advisor: Richard H. Kemp, Materials and Structures Division NASA Lewis Research Center, Cleveland, Ohio

16. Abstract

An analysis method termed TEJ-JET is described whereby measured transient elastic and inelastic deformations of an engine-rotor fragment-impacted structural ring are analyzed to deduce the transient external forces experienced by that ring as a result of fragment impact and interaction with the ring. Although the theoretical feasibility of the TEJ-JET concept has been established, its practical feasibility when utilizing experimental measurements of limited precision and accuracy remains to be established. This document describes work in progress to make that assessment.

The experimental equipment and the techniques (high-speed motion photography) employed at the Naval Air Propulsion Test Center to measure the transient deformations of fragment-impacted rings are described. Sources of error and data uncertainties are identified. Techniques employed to reduce data reading uncertainties and to "correct" the data for optical-distortion effects are discussed. These procedures, including spatial smoothing of the deformed ring shape by Fourier series and time-wise smoothing by Gram polynomials, are applied illustratively to recent measurements involving the impact of a single T58 turbine rotor blade against an aluminum containment ring. Plausible predictions of the fragment-ring impact/interaction forces are obtained by one branch of this TEJ-JET method; however, a second branch of this method, which provides an independent estimate of these forces, remains to be evaluated in near-future studies. These two estimates of these "externally-applied forces", each with an appropriate "reliability factor" will then be combined in a Kalman filter branch of the TEJ-JET process to provide an "optimum estimate" of these fragment-ring impact/interaction forces.

17. Key Words (Suggested by Author(s))		18. Distribution Statement
Turbojet Rotor Containment Aircraft Hazards Aircraft Safety Experimental Methods High-Speed Photography Error Assessment	Data Smoothing Techniques Transient Structural Response Large Deflections Elastic-Plastic Behavior	Unclassified, Unlimited

19. Security Classif. (of this report): Unclassified	20. Security Classif. (of this page): Unclassified	21	22

* For sale by the National Technical Information Service, Springfield, Virginia 22151

FOREWORD

This report has been prepared by the Aeroelastic and Structures Research Laboratory (ASRL), Department of Aeronautics and Astronautics, Massachusetts Institute of Technology, Cambridge, Massachusetts under NASA Grant No. NGR 22-009-339 from the Lewis Research Center, National Aeronautics and Space Administration, Cleveland, Ohio 44135. At the Lewis Research Center, Mr. Patrick T. Chiarito and Mr. Solomon Weiss served as technical monitors and Mr. Richard H. Kemp served as technical advisor. The valuable cooperation and advice received from these individuals is acknowledged gratefully.

The authors wish to acknowledge the cooperation, advice, and assistance of Messrs. G.J. Mangano and R. DeLucia of the Naval Air Propulsion Test Center, Philadelphia, Pennsylvania. These individuals worked diligently to develop and improve the experimental techniques involved in this effort. Mr. Mangano also has reviewed this report and has generously contributed constructive suggestions for improving its content and clarity.

CONTENTS

CONTENTS CONCLUDED

LIST OF ILLUSTRATIONS

LIST OF ILLUSTRATIONS CONCLUDED

SUMMARY

The need for rational structural design methods to design structures for either containing or deflecting (into "harmless" regions) engine rotor fragments from aircraft jet engines is discussed. It is argued that efficiency and convenience considerations lead one to employ two-dimensional rather than shell and/or three-dimensional-solid structural analysis models at this time. Further, the judicious use of both theoretical analysis and experimental data on engine-rotor-fragment impact with selected structures is essential to achieve reliable and efficient designs for this complex problem since only a limited understanding of its many aspects currently exists.

Accordingly, restricting attention to fragment containment/deflector structures whose deformations are confined essentially to one plane (the plane of the structural ring), it is noted that already-validated methods for predicting the large-deflection elastic-plastic transient deformations of such structures are available; reliable and accurate predictions result, provided that one has accurate knowledge of the externally-applied transient forces to which the structure is subjected. In the present context, these forces are the forces applied to the structural containment/deflector ring by the impacting fragment(s) during the impact and interaction process. A means for estimating these impact/interaction forces experienced by the "ring" is to conduct experiments in which (a) selected types of engine-rotor fragments are caused to impact "typical" rings and (b) careful measurements are made of the transient response and deformation of the impacted structure. The information is then used in a "backward-solution" of a JET structural response computer code to obtain an estimate of the externally-applied forces which must have produced the experimentally-measured transient motion and deformations of the fragment-impacted ring; this procedure is termed the TEJ-JET process.

SUMMARY CONCLUDED

The intent is that relatively few experiments used in conjunction with the TEJ-JET process will provide information on the external forces experienced by a containment ring to a given type of fragment attack such that computer code studies of containment-structure response could be carried out to reduce greatly the number of experiments required for a wholly-experimental study of the engine-rotor-fragment containment/deflection problem.

The theoretical feasibility of the TEJ-JET process was established earlier. The present report describes work in progress to assess whether or not this scheme is feasible in a practical sense when experimental transient deformation data of the limited precision and accuracy provided by currently-available techniques are employed.

Discussed here are the high-speed photographic techniques, the film reading techniques, and supplementary measurements employed at the Naval Air Propulsion Test Center to obtain the desired transient response data. Sources of error and data uncertainties are identified. The techniques employed to reduce data reading uncertainties and to "correct" the data for optical-distortion effects are discussed. These procedures, including spatial smoothing of the deformed ring shape by Fourier series and timewise smoothing by Gram polynomials, are applied illustratively to recent transient response measurements involving the impact of a single T58 turbine rotor blade against an aluminum containment ring. Plausible predictions of the fragment-ring impact/interaction forces are obtained by one branch of this TEJ-JET method; however, a second branch of this method, which provides an "independent" estimate of these forces, remains to be (but will be) evaluated in near-future studies. These two estimates of these "externally-applied forces" each with an appropriate "reliability weighting factor" will be combined in a Kalman filter branch of the TEJ-JET process to provide an "optimum estimate" of these fragment-ring impact/interaction forces.

SECTION 1

INTRODUCTION

1.1 Background

The occurrence of potentially dangerous failures of high-speed rotating parts in aircraft turbojet engines has been well documented in the past, and remains a problem without an adequate solution to date (Refs. 1 to 3). Fragments emanating from high-speed turbine, fan, or compressor rotors, be they blades or portions of the disk with attached blades, may threaten passenger safety and cause damage to equipment if not deflected away from vital components or fully contained.

The design and construction of over-strong turbine parts to eliminate the possibilities of failure are uneconomical, since the possibilities of overspeed, overheating, fatigue, and the ingestion of foreign objects cannot be avoided entirely and may precipitate a failure. Diverting some of the weight penalty into the design and construction of a heavier engine casing or additional protective structure around failure-prone regions to contain or deflect the fragments may become acceptable with the realization that turbojet rotor failures cannot be eliminated completely. Hence, the problem of analytically and experimentally studying the interaction of fragments impacting containment/deflection structures is an important one.

Since mid-1968, the Aeroelastic and Structures Research Laboratory of the Massachusetts Institute of Technology (MIT-ASRL) has been investigating for NASA-LeRC theoretical methods of studying the fragment containment/deflection problem, with the primary objective being to develop the necessary analytical tools and associated computer programs which could be used by industry to aid in the process of designing containment/deflection structures for

turbojet engines (Refs. 4 to 10). An experimental effort (Refs. 11 to 15) has been carried out by the Aeronautical Engine Division of the Naval Air Propulsion Test Center[+] (NAPTC), Philadelphia, Pa. A closely-coordinated exchange of ideas, research developments, and suggestions for future programs has mutually aided these theoretical and experimental efforts.

Theoretical methods of analysis can play many useful roles in the search for and the determination of practical least-weight design of structures for containing or deflecting engine rotor fragments.

For preliminary design, it is often useful to employ a severely simplified model to approximate the behavior of candidate containment/deflection structures. In particular, one might approximate the actual containment structure which undergoes three-dimensional deformation under fragment attack by a structural ring which undergoes essentially only planar (2-d) deformations. This simplification carries with it both advantages and limitations. Some of the advantages are that this approach provides a very efficient way for (1) conducting preliminary estimates for containment vessel thickness (compared with using a general 3-d shell analysis), (2) screening candidate containment materials to assess their comparative efficiencies, (3) exploring the effects of various approximate forcing functions, and (4) determining approximately the forces applied to the containment vessel by attacking fragments via theoretical analysis alone and/or by appropriately combining experiment and theory. However, the use of such a method will not enable one to predict reliably the required threshold containment thickness of an actual containment vessel -- the absolutely essential 3-dimensional shell deformation ingredient is missing: a quantitative assessment of the importance of this ingredient remains to be made but recent NAPTC parametric test results clearly show its importance.

[+]To be relocated shortly at Trenton, New Jersey.

For detail design purposes, one needs more refined estimates of required containment vessel thickness than the aforementioned simplified analysis can provide. This information can be most effectively furnished by a coordinated program of experiments and more comprehensive structural analysis. The structural analysis (and also experiments) must include more comprehensive modeling of the actual structural configuration, material properties, and the 3-d shell deformation behavior. Proven analysis methods of this type would be useful for (1) assessing the adequacy of the design under a series of forcing functions which are chosen to represent various likely and/or critical types of fragment attack and (2) reducing the amount of ad hoc testing. However, the present knowledge of the forcing function(s) applied to containment structures during fragment attack is poor; this represents a major source of difficulty and uncertainty.

Accordingly, rather than plunging into the very complex problem of analyzing and predicting these forcing functions for the general problem of a 3-d containment/deflection shell under attack by a simple single fragment, a complex single fragment, or a complex succession of fragments, it was decided to concentrate effort first on the much simpler problems of a planar containment vessel (a structural ring) in order to develop:

(a) methods for estimating the attendant forcing functions (by theoretical analysis alone or by a combination of theory and experiment) and/or

(b) methods for predicting the ring/fragment interaction and structural response directly without seeking an explicit evaluation of the forcing function itself.

Various approaches to items (a) and (b) have been considered. The TEJ-JET concept (Ref. 5) was proposed for item (a); see Section 2 for a description of the essence of this method. Also, the use of energy and momentum conservation relations for the fragment/ring system was considered for items (a) and (b) -- the respective resulting schemes are labeled CFM-JET (Ref. 8) and CIVM-JET (Ref. 7), respectively. The following terse key-word description identifies the principal advantages and disadvantages of these three approaches:

- TEJ-JET
  - Applicable to Simple Single as well as Complex Multiple Fragments
  - Must have Measured Transient Structural Response Data
  - Predicted Transient Externally-Applied Loads are Useful for Preliminary Design
    - Use as Unchanged in Screening Calculations for Various Containment Vessel Materials

      or

    - Conduct Spot Check Tests and TEJ-JET Analysis for One or Two Other Materials
- CIVM-JET AND/OR CFM-JET
  - Does Not Require Measured Transient Response Data
  - Uses Basic Geometry, Material Property, and Initial Condition Data
  - Readily Applied to Single Fragments
  - Multiple or Complex Fragments
    - More Difficult to Apply
    - Needs Further Development; Complex Logic
  - Complex but has Much Potential for Future

Because of the potential of the TEJ-JET concept for determining "representative forcing functions" for both simple fragments and very complex fragments with apparently comparable effort, and because of limited funds and available trained personnel, it was decided to pursue the TEJ-JET concept first -- deferring action on these alternate approaches until an appropriate later time. Accordingly, the development of the TEJ-JET concept has proceeded, with the first stage of development (Ref. 5) being devoted to containment rings subjected to single blade impact; NAPTC Tests 88 and 91 were conducted in an effort to obtain the required experimental data. Analyses of these data have indicated the necessity for improved experimental measurements. Hence, NAPTC subsequently has carried out similar tests with improved techniques.

The recent MIT-ASRL work on the analysis, evaluation, and application of the experimental results relating to the TEJ-JET concept is the central topic of the present report. Similar containment ring experiments and TEJ-JET analyses involving (a) a tri-hub T58 turbine rotor impact and/or (b) a single blade failure from a fully-bladed rotor followed by subsequent impacts and additional blade failures have been recommended in an effort to define typical forcing functions for additional possible and/or likely types of fragment attack. It will remain, however, to be demonstrated whether adequate rules can be devised to "extrapolate" this forcing-function information to represent similar types of fragment attack (with perhaps different fragment material properties) against containment vessels composed of material different from that used in the aforementioned experiments.

It is to circumvent this tenuous extrapolation problem and to eliminate the necessity for making the detailed experimental transient response measurements now required for the TEJ-JET concept that effort has been devoted to developing

other fundamental analysis procedures which will drastically reduce the requirements for detailed experimental transient response measurements of containment vessels subjected to fragment attack. The attendant analysis procedures are termed CIVM-JET (Ref. 7) and CFM-JET (Ref. 8).

The information flow chart shown on the next page indicates schematically the roles of the JET structural response computer codes in relation to the concepts TEJ, CIVM, and CFM.

In the information flow chart shown on the next page, reference is made to computer programs JET 1, JET 2, and JET 3 -- each with various different capabilities. The computer programs JET 1, JET 2, and JET 3 enable one to predict the large deflection elastic-plastic transient structural responses of simple 2-d planar structures such as rings to prescribed* externally-applied forces and/or to prescribed* imparted velocities. JET 1 (Ref. 4) pertains to free single-layer rings which may be subjected to mechanical and/or thermal loads, whereas JET 2 (Ref. 5) applies to both single-layer and multilayer, multimaterial, hard-bonded unheated free rings which may be subjected to mechanical loads and/or prescribed imparted velocities. JET 3 (Ref. 9) applies to both complete and partial unheated single-layer rings which can be either free or restrained in various ways; prescribed mechanical loading or imparted velocities may be employed. References 4, 5, and 9 may be consulted for further details.

The present report is concerned mainly with documenting the experimental techniques employed in obtaining transient deflection data, the subsequent analysis, improvement, and evaluation of this data, and its preparation for use by the TEJ-JET method for determining from measured ring transient structural response data the external forces applied to a containment/deflection ring during ring/fragment impact and interaction.

*The key item of present interest is that these quantities must be prescribed or known.

EFFECTS ON CONTAINMENT RINGS
FROM ROTOR-DISK FRAGMENT IMPACT

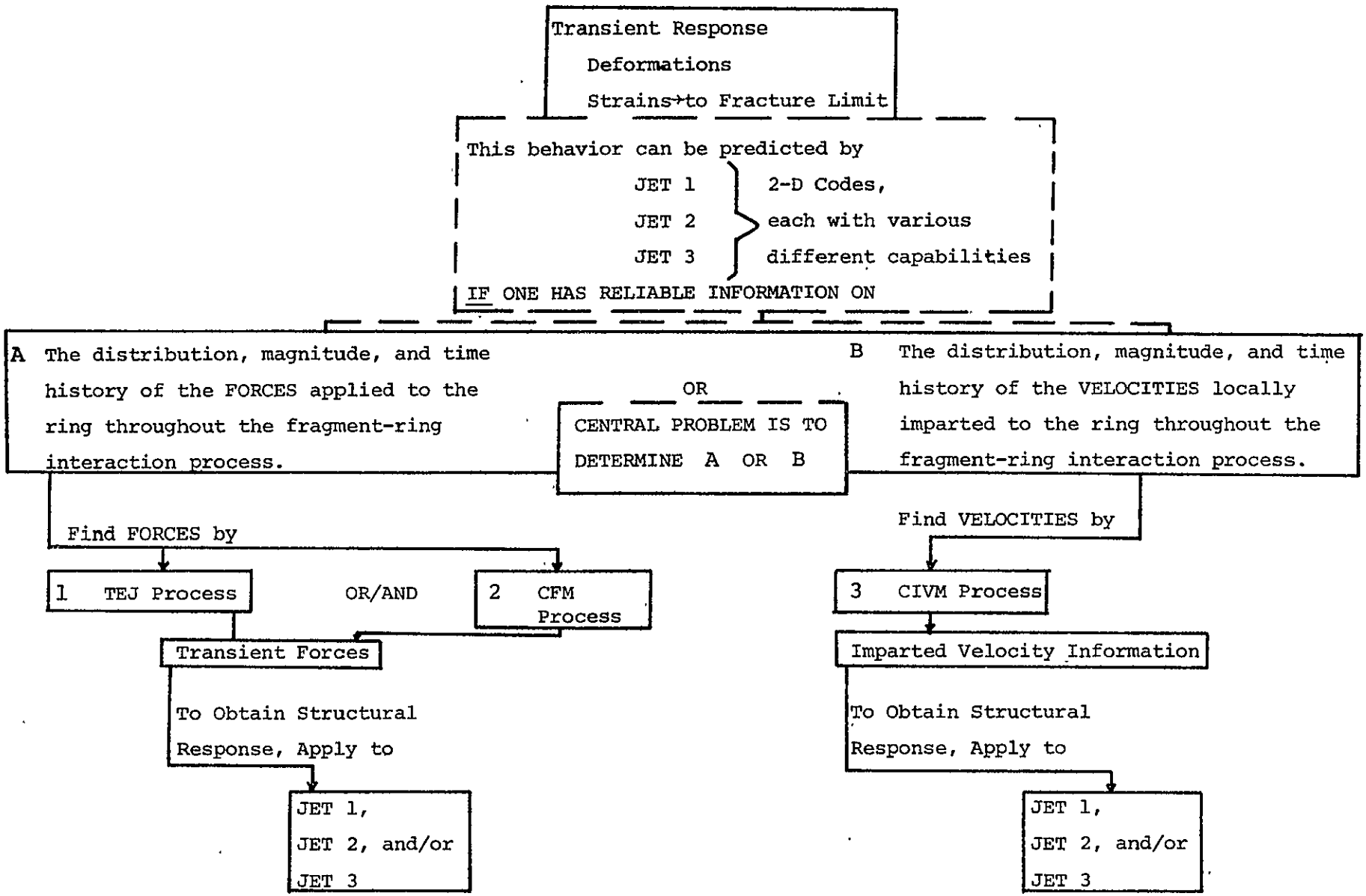

Finally, the following key-word comments on the principal roles which experiments are considered to play in the engine rotor fragment containment/deflection problem may be useful:

E.1 Explore Phenomena

- Simple Cases
- Very Complex Cases (too complex to analyze reliably by available methods)

E.2 Data to Test Analysis Methods and Aid Development

E.3 Preliminary Data to Guide Designers

- Simple Rings (2-d structure): LOGICAL STARTING POINT
  - Selected Fragments and Conditions
  - Assured Containment
- Simple Cylindrical Shells (more variables)
- Ring-Stiffened Shells (many more variables)

E.4 "Proof Tests" of Full-Scale and/or Part-Scale Designs

- Conditions for Meaningful Proof Test
  - Fragments
    - Types (most critical and/or likely)
    - Sizes (most critical and/or likely)
  - Temperature Simulation: Takeoff
  - Pressure (Air Flow, etc.): Takeoff

This report deals with item E.2.

The NAPTC experiments (Refs. 11 through 15) have been and are in the process of contributing particularly to item E.1, E.2, and E.3, with the contribution to item E.2 being pertinent to the TEJ-JET, CIVM-JET, and CFM-JET developments.

1.2 Report Organization and Contents

As noted earlier, the computer programs JET 1, JET 2, and JET 3 can provide accurate predictions of large-deformation elastic-plastic transient responses of containment/deflection rings if one supplies accurately prescribed information on the externally-applied transient forces (or velocities imparted) to the ring by the attacking fragment. However, the knowledge of the transient forces has been poor. As a step toward improving that knowledge, the TEJ-JET concept and the associated computer program which can be employed to predict the location, magnitude, and time history of ring/fragment interaction forces, based on experimentally measured containment ring deflection history data, have been pursued. The application of this type of analysis is intended to provide insight into the types of forcing functions that occur typically; such forcing functions subsequently can be employed in the JET programs for carrying out parametric calculations of design interest for various simple containment/deflection structures. However, securing suitably accurate containment ring displacement history data (the necessary input information for the TEJ-JET analysis) requires a carefully controlled and conducted experiment wherein high-speed motion pictures of a fragment-attacked containment structure are taken, from which the displacement history can be evaluated.

The contents of the remainder of this report consist of the following. Section 2 pertains to the TEJ-JET analysis procedure, with the presentation of the concept, the capabilities, and the limitations, and establishes the input requirement of reliable experimental data on the space-time history of the containment ring deformations to be used for the prediction of reliable forcing functions. Section 3 is devoted to the discussion of the NAPTC fragment containment/deflection experimental program, describing the objectives, the test equipment,

the experimental technique, and the recording and reduction of the data. In Section 4, the NAPTC experimental data are analyzed, the sources of error are identified, and the processing employed to improve the accuracy, reliability and usefulness of the data is described. Section 5 presents the specialized subprograms which are needed for the analysis of the experimental data and the preparation of the data for use in the TEJ-JET program, and describes the functions they serve. Section 6 is devoted to the applications of the specialized subprograms, presenting the available data, the magnitudes of the errors in the experimental data, the compensation for optical distortions, the smoothing techniques employed in preparing the data for use in TEJ-JET, and the exercising of the different steps of the program with sample experimental data for the estimations of the interaction forces by different approaches. Finally, Section 7 summarizes the report and presents some comments.

SECTION 2

THE TEJ-JET CONCEPT

Although the TEJ-JET concept is theoretically valid for very general structural response problems, attention is restricted herein (as motivated in Section 1) to 2-d structural response problems; the structure may undergo large-deflection elastic-plastic transient structural behavior but the deformations are all considered to lie, essentially, in one plane.

For problems of this type, structural response prediction codes of the finite-difference type (JET 1 and JET 2) and of the finite-element type (JET 3) have been developed at the MIT-ASRL. It has been demonstrated that these codes can provide accurate large-deflection elastic-plastic transient response predictions for structural rings (a) whose material properties are known and (b) which are subjected to (1) a known distribution and time history of externally-applied forces or (2) a given distribution and time history of velocity increments. Conversely, then, if one has detailed information of the transient structural deformations and motion of a given structural ring, one should be able, in principle, to "carry out a backwards solution" to determine the distribution and time history of the externally-applied forces (and/or velocity increments) which were responsible for producing the "observed transient structural response"; this idea is the essence of the TEJ-JET concept.

In the present context, the TEJ-JET approach involves making very detailed experimental measurements of the motion of a structural ring subjected to rotor fragment attack. The subsequent TEJ-JET processing of this information provides the spatial distribution and time history of the externally-applied forces which the ring experiences from fragment impact and interaction with the ring.

The theoretical feasibility of the TEJ-JET concept has been verified by carrying through examples wherein a structural ring of known properties has been subjected to a prescribed distribution and time history of external forces. The resulting structural response was predicted by a JET code. This structural response information was then processed (a) before and (b) after having been altered by imposing random errors with a zero mean but various levels of probable error to simulate "experimental observation and data reduction errors"; the resulting TEJ-JET predictions of the externally-applied forces were in excellent agreement with the known externally-applied forces (Ref. 5).

Therefore, it was believed to be timely to apply the TEJ-JET analysis to experimentally-observed transient deformation and motion data for a fragment-attacked containment ring in order to deduce the spatial and timewise history of the external forces which the ring had experienced as a result of fragment impact. In order to minimize experimental and data interpretation uncertainties, the initial studies have involved the impact of only a single T58 turbine rotor blade against "initially circular" containment rings of 2024-T4 and 6061-T6 aluminum chosen because of their well known stress-strain behavior. For this study only one blade was on the rotor -- to avoid the complexity of subsequent blade/blade impacts of the "thrown blade" with the remaining blades on a usual T58 rotor.

From the earlier noted studies, it is clear that the TEJ-JET concept is feasible from a thoretical viewpoint, provided that one has available sufficiently accurate and complete transient structural response information on the fragment-attacked ring. Experimentally determined structural response data, however, involve many possible sources of error and uncertainty. It remains, therefore, to determine whether or not available experimental observation/recording techniques and modern data processing techniques are adequate to provide transient response

data of quality and detail sufficient to permit deducing reliably the impact-induced externally-applied forces suffered by the subject fragment-containment ring. This is the central matter which is being addressed in the present report.

Preliminary studies had shown that early experimental and data reduction techniques did not provide transient structural response data of adequate[+] quality for this purpose. Hence, improvements in both experimental techniques and in data reduction/processing techniques were devised and employed. The lessons learned in this process are discussed in subsequent sections of this report; in particular, discussed are the ways and means employed in the effort to better the quality of the data required as input in the TEJ-JET program: (1) by improvements in the experimental techniques in obtaining high-speed motion pictures of the fragment-ring interaction in a spin chamber, (2) by careful readout of the ring position data from individual picture frames, then (3) by analyzing the data to determine sources of error and introducing compensating corrections, and (4) finally smoothing the transient response curves analytically, prior to application in the TEJJER segment (see Fig. 3) of the TEJ-JET program.

It should be emphasized that the main purpose of the TEJ-JET scheme is to obtain estimates of the distribution and time history of the external forces experienced by the containment (or deflector) structure arising from a succession of impacts from one or more simple or complex fragments. As depicted in the diagram on the following page, one analyzes measured transient structural response data of the containment structure via TEJ-JET processing to deduce the externally-applied forces which must have produced the observed transient structural response. The intent

[+]In fact, one could not deduce from those data even "plausible-looking" transient externally-applied forces.

TEJ-JET INFORMATION FLOW

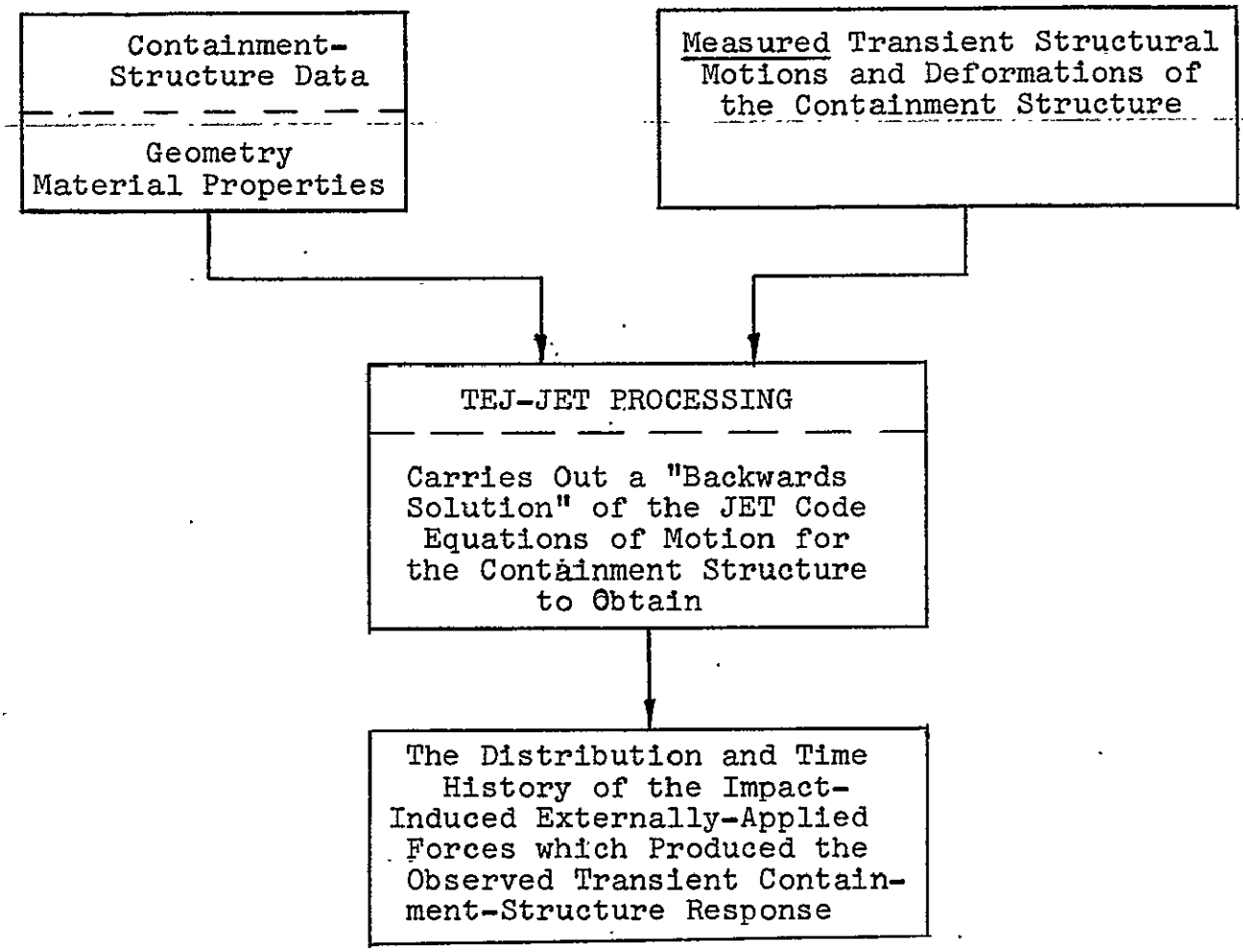

is that if the TEJ-JET type of analysis were applied to typical cases of, for example, (a) single-blade impact, (b) disk-segment impact, and/or (c) multi-bladed disk fragment impact, one could determine the distribution and time history of the forces applied to the containment ring for each case. Such forces (or appropriate modifications thereof) could then be applied tentatively in computer code parametric studies to estimate the structural response for a variety of containment materials for containment rings subjected to similar fragment attack. For structural/material cases differing from that used in the postulated experiment from which TEJ-JET has extracted forcing-function information, one could be guided in appropriately modifying these external forces by dimensional analysis considerations and selected spot-check experiments that otherwise would be needed in a wholly-experimental attack upon the engine rotor fragment containment/deflection problem. Additional reasons for pursuing the TEJ-JET idea are given on pages 4, 5, and 7 of this report.

SECTION 3

FRAGMENT CONTAINMENT EXPERIMENTS

3.1 Objectives

Since 1963 the Aeronautical Engine Laboratory (now the Aeronautical Engine Division) of the Naval Air Engineering Center (now the Naval Air Propulsion Test Center), Philadelphia, Pa., has been engaged in a Rotor Disk Burst Protection study sponsored by the Lewis Research Center of the National Aeronautics and Space Administration. The initial objective of the study was to determine experimentally the feasibility of containing or deflecting fragments of burst rotors from turbojet aircraft engines with the aim of preventing injury to passengers and crew or catastrophic loss of aircraft.

In pursuing this goal an experimental program was developed to generate data useful for the design of containment/deflection devices with acceptable weight penalties. This included the design and development of a Containment Evaluation Facility where fragments from intentionally-failed rotors could interact with a containment/deflection device in a spin chamber, and the interaction history could be recorded by high-speed motion picture photography and strain measuring systems. The facility has been used extensively for the development of test techniques, the evaluation of containment/deflection systems, and parametric testing. References 11 to 15 may be consulted for more detailed information.

With the need to understand the mechanics of the interaction between the fragments and the containment/deflection device, the objectives of determining the interaction forces, their duration and spatial distribution, as well as the penetration or failure modes were stated. To accomplish this, the need to develop computer programs with appropriate mathematical

models for the interacting systems and adequate input conditions was apparent. This analytical investigation was undertaken by and carried out at the Aeroelastic and Structures Research Laboratory (ASRL) at M.I.T.

This report deals with one phase of the analytical investigation carried out at the ASRL --- that of determining the actual interaction forces, both spatially and temporally. Although the developed program is conceptually capable of treating complex interaction cases, for the initial investigation and validation purposes the much simpler case of a single blade interacting with a circular containment ring was considered. The necessary input information of ring deflection history has been and will be provided by experiments carried out at the NAPTC. The objective was to carry out carefully-controlled experiments where a single blade from a T58 turbine rotor (with all other blades removed from the disk) was caused to fail at a nominal preselected speed and to impact and interact with an aluminum alloy ring of known dimensions and material properties (such as 2024-T4 or 6061-T6 aluminum alloy). The resulting few milliseconds of interaction were recorded by high-speed motion picture photography in an attempt to provide high quality pictorial records of the ring deflections. This pictorial record would then provide the numerical data: the Cartesian coordinates for specific points on the containment ring as a function of time. Assembling the sets of position components from the sequence of pictures resulted in the sought position-versus-time history of the containment ring; this constitutes the input data to the TEJ-JET analysis.

3.2 Test Equipment

For the single-blade containment tests outlined above, the larger of the two spin chambers at the Rotor Spin Facility of the NAPTC was used. This chamber has an inside diameter of 157 inches and can be evacuated to maintain a pressure of 50

microns absolute. A protective liner, made of concentric steel cylinders laminated and bolted together with an inside diameter of 120 inches, provides protection for the chamber walls from fragments generated during destructive tests. The chamber is equipped with photographic/observation ports around its circumference away from the plane of possible impact from fragments of a failed rotor. With an optical quality mirror placed at a 45-degree angle from the vertical under the rotor and ring test assembly, a "bottom view" in the axial direction of the rotor (spinning in a horizontal plane) is provided through a photographic observation port.

The interaction of blade and containment ring is recorded by a high speed continuous framing camera positioned at the port. The camera, a Beckman and Whitley Model 350, is capable of producing a sequence of pictures at a framing rate of up to 35,000 pictures per second on a 35 mm film strip approximately 34 inches long. The film is mounted on a rotating drum transport which revolves at a speed of 9375 rpm at the maximum framing rate. The framing shutter is a set of rotating mirrors which expose the sequence of pictures on alternate halves of the film width, with the exposures on one half of the film lagging in position 14 frames behind pictures exposed on the other half of the film.

The photo lighting unit, a Beckman and Whitley Model 358 Electronic Flash designed for use with the camera described above, has a maximum setting to provide 6,000,000 peak beam candle power for a pulse duration of approximately 2.7 milliseconds. Rise time for the flash is within 1.5% of the pulse duration, and extinction time is within 4% of the pulse duration. The flash can be triggered through a voltage pulse, a closing contact switch, or an opening contact switch. There is a maximum delay of 50 microseconds between triggering and

initiation of the light pulse. Different methods of triggering the flash were attempted in an effort to obtain a few pictures prior to fragment-ring contact.

The test rotor is attached to the driveshaft of a drive-turbine powered by compressed air. The test assembly is suspended from the bottom of the spin chamber lid, and may rotate the test rotor in a clockwise or counterclockwise direction in the horizontal plane. The containment ring is positioned concentrically with the rotor and in the same plane, resting on top of and supported freely by three thin guy wires radiating outward from the center of the ring; frictional forces between the ring and the support wires are deemed negligible. A complete freely-supported ring is used because (among other reasons) this configuration is well-defined in terms of "boundary conditions" for structural response analysis purposes.

Containment rings were machined from billets of 2024-T4 or 6061-T6 aluminum. The ring dimensions were: inside diameters of 15.0 inches, radial thicknesses of approximately 0.15 inches, and axial lengths of approximately 1.5 inches. The edge of a ring, in view of the camera, was marked with reflective paint at 72 equidistant stations (five degrees apart) to represent the ring "mass points" whose position-versus-time history was to be recorded. A stationary background plate with reference points* was employed to provide an inertial reference frame for each individual picture exposed on the film strip. Figure 1 depicts the experimental set-up as viewed by the camera, showing the reference grid, the ring "mass point stations" and the blade reference marks.

The pictorial record of the ring deflection history is translated into numerical ring "mass point" position data by projecting an enlarged image from each frame of the motion

*The number and location of reference points were altered in later tests to improve the reliability and/or accuracy of the reference frame and provide a known gridwork to be used in checking for possible image distortions.

picture film on a screen and reading the Cartesian position coordinates of the reference points, the ring "mass points", and reference marks on the blade. The film reader is a Nuclear Research Instruments Corp. combination motion-picture projector and precision measuring device. It can accommodate film strips up to 70 mm. wide, which can be projected onto a 24x24-inch ground-glass projection screen, magnified 10 times or 50 times by using the appropriate lens system. The image on the projection screen moves along with the motion of the film carrier, while the reticle cross-hairs remain fixed at the center of the screen. Thus, the data point image is brought to alignment with the cross-hairs by moving the film carrier. As the film carrier is moved in the x,y directions in the plane of the film, digital disc encoders on the lead screws provide the position coordinates; the nominal screw pitch is 1 mm, and with a 1000-count encoder the smallest position increment is 1 micron. An IBM 026 card punch connected to the system keypunches the position coordinates on punch cards in a predetermined format for subsequent analysis.

3.3 Experimental Technique

The generation of experimental data for use in an exacting analysis necessitates careful controls of the conditions under which the experiments are carried out and the employment of techniques which will insure the maximum reliability of the generated data.

Frequent feedback between the NAPTC, where the experimental effort was carried out, and MIT-ASRL, where the analysis of the experimentally-obtained data was carried out, resulted in continuous reassessment of the methods employed and indicated the ways and means to obtain improved results.

For the full-scale containment tests carried out at the NAPTC in support of the TEJ-JET analytical effort, T58 turbine rotors were employed. All blades, except one, were re-

moved from the turbine disk, and the single remaining blade was appropriately weakened at the root to cause its failure at an approximate predetermined rotational speed. The turbine was then balanced dynamically and mounted on the driven shaft of the spin chamber turbine drive system. In the later tests, reference markings were added on the single blade for ease of accurately locating its trajectory prior to and subsequent to impact with the containment ring. These reference markings were in the form of four narrow bands (chordwise on the blade) of black paint. One of the bands was at the tip of the blade, thus outlining the edge which would be first in contact with the containment ring. The other bands were at known stations between the root and the tip of the blade. One could thus identify "blade reference points", say at the leading and trailing edges of the blade on centerlines of the reference bands, the position-time history of which would determine the trajectory, orientation, and speed of the attacking blade (see Fig. 1). As the blade contacted the containment ring and then deformed, a reduced number of "blade reference points" stayed visible, as illustrated, for example, in Fig. 2.

The containment rings employed were cut from aluminum alloy billets and machined to specific sizes. Initially 2024-T4 aluminum alloy was the material used. In the later tests 6061-T6 aluminum alloy material was used. The uniaxial mechanical (elastic-plastic stress-strain) properties of the containment rings are well known from standard tests. However, very few static uniaxial stress-strain tests of the actual material used were carried out to determine compliance with the "standard" properties.

Machining a ring of 15-inch internal diameter and 1.5 inch axial length to a thickness of approximately 0.15 inches is inherently a difficult task. Although uniformity of cross-sectional dimensions (thickness and axial length) and radial distance was sought, slight oblateness in the circular shape of the ring

and some variation of thickness within a known tolerance is inescapable. Hence, in the latter tests the dimensions of the machined ring were carefully recorded; in particular, the ring thickness at specific stations along the perimeter was measured.

The containment rings were also marked to identify 72 equidistant points (5 degrees of arc) around the perimeter. These points represent the so-called "mass point" stations the position-versus-time history of which is needed for analysis. For the initial tests, the "mass points" were marked by masking off sections on one edge of the ring before applying black paint, thus exposing the more reflective aluminum surface alternating with the black sections. In later tests, the contrast was enhanced by applying reflectorized paint at the "mass point" locations on the ring. An additional marking at one point between the equidistant "mass point" positions gave an origin reference for the consecutive numbering of the mass points for identification purposes in the motion pictures (see Figs. 1 and 2).

Positioning of the containment ring in the same horizontal plane as the test rotor, and concentric with it, was done with spacer gage blocks. The set of support wires on which the containment ring rested was adjustable for the vertical positioning of the ring in the proper plane. Friction of the ring on the support wires maintained the concentric positioning of the ring around the test rotor.

The background plate was, by necessity, placed above the ring-rotor assembly plane. As the photographed view was the bottom view of the test assembly, the background plate then became positioned in a plane parallel to but beyond the plane of the ring-rotor assembly. This point is noted to stress the fact that the ring "mass point" markings, which were on the

viewed edge of the ring, and the reference points which were marked on the background plate, were not on the same plane and hence were at a different focal distance from the camera. The effect would be a slight reduction in sharpness of focus and a slightly different magnification factor for the two different planes; this reduction was not evident because of the depth of field.

For the initial tests, the reference marks on the background plate were placed at four locations roughly forming the four corners of a square. In addition, at each location a set of a few intersecting lines was used, thus providing a gridwork, any points of which could be picked as an inertial reference point. For the later tests, after due experimentation and analysis, a new reference-point pattern was designed and used on the background plate. These reference points were carefully placed at known locations and in sufficient numbers to provide a background gridwork which could be used not only to determine an inertial frame of reference, but also could provide a basis for checking magnification factors in different directions and regions of the field of view on the film plane, and hence identify possible optical distortion in the circumferential or radial directions of the resulting pictures. The reference point gridwork was a pattern of three points on each of eight radial lines (45 degrees of arc in separation) with the inboard set of points at a radial distance of 6.5 inches, the central set at a radial distance of 8.5 inches, and the outboard set at 9.5 inches. The points were actually drilled on the background plate, and outlined with a circular band of reflectorized paint for visible contrast. The rest of the background plate was painted in flat white. A black backup plate behind the reference plate was visible through the reference point holes. The result is shown typically in Figs. 1 and 2.

With the above test set-up in the spin chamber, the chamber was sealed and evacuated, and the single-bladed test rotor brought up to speed. Simultaneously, the high-speed motion-picture camera was accelerated to its predetermined framing speed. Upon the failure of the single blade at its weakened root, the electronic flash was triggered and the film was exposed with a sequence of frames showing the interaction between the containment ring and the attacking fragment. Because of the finite rise-time of the flash to peak output and inherent delays in switching circuitry to initiate the flash, it was found that triggering the flash upon impact of the blade with the ring caused the initial instants of the interaction to go unrecorded. Also, the actual time of initial impact was difficult to determine. Accordingly, a triggering mechanism which initiates the flash upon the separation of the blade from the disk (thus breaking a circuit) was designed and used, thus providing a few picture frames prior to impact, in addition to the ensuing interaction record. The duration of the flash before light output decay was ample to record the interaction period of interest.

The high-speed motion pictures were exposed on Kodak Tri-X film. Normal developing techniques were used for the film strip. Enlarged prints of each picture frame were made as a visual record of the sequence of events. Initially, to safeguard the original negative, positive transparencies were made (contact printed) and used for data reduction in the film reader. However, the original negative itself was used in later cases as a more reliable record for data reduction.

The film reader holds the film on a carriage between two layers of glass. The carriage can be moved in the horizontal plane and its position (Cartesian x-y coordinates) is automatically shown on a panel in digital form in microns. The same information can be automatically keypunched in specific fields of a punch card.

The projected image of the negative film is reflected via an optical quality mirror, set at 45 degrees from the vertical, onto a ground glass rear-projection screen, mounted vertically. An image, magnified 50 times, is thus seen, superposed by a stationary image of a set of cross hairs. Thus, the x-y coordinates of any point on the film can be obtained by moving the film carrier such that the point in question lies at the intersection of the cross hairs. With the knowledge of the Cartesian coordinates of all the background reference points, ring "mass points", and the blade reference points obtained in the film reader axis system, the relative positions of all points are known. It is imperative, of course, that the position of the film relative to the carriage remain fixed while all points on each picture frame are being read. A simple transformation will then cast the position of all points in an "inertial reference frame" based on the reference (background) points appearing in each picture.

To insure against the possibility of inadvertently recording the wrong coordinates for a point and to increase the reliability of the position data, the sequence of reference points, mass points, and blade references was read a total of four times for each picture.* An averaged reading would thus be more indicative of the point positions, and any gross error in one reading would be identified if it fell beyond a certain tolerance away from the average of the others. Should the latter happen, this "bad reading" would be discarded in computing the average reading.

*By using n repeated readings of any given position, the reliability of that position determination is increased by $\sqrt{n}$; in this case where n = 4, the reliability is increased by a factor of 2.

SECTION 4

ANALYSIS OF EXPERIMENTAL DATA

4.1 Possible Error Sources

The experimental high-speed motion picture data obtained by the NAPTC in the cited specialized single-blade containment tests for subsequent analysis by the TEJ-JET program of the MIT-ASRL are limited in accuracy by many error and uncertainty sources. These sources intervene at many stages between the initial design of the test set-up and the final desired record of numerical data which consists of the Cartesian inertial-space coordinates of (1) the background reference points, (2) the ring "mass point" stations, and (3) the blade reference marks, for each individual picture from the high-speed motion picture film.

The error and uncertainty sources may be grouped conveniently into the following categories:

(a) data point position uncertainties,
(b) film reading and resolution uncertainties, and
(c) optical distortion effects.

Each of these categories is discussed in Subsections 4.2, 4.3, and 4.4, respectively. Subsection 4.5 presents the spatial and timewise smoothing techniques employed to compensate for the random errors.

4.2 Data Point Position Uncertainties

Falling into this category would be the case of an out-of-round containment ring, marked with the 72 "mass point" stations at the viewed edge. Difficulties inherent in machining a relatively thin and short (in the axial direction) ring, discussed earlier, have in fact resulted in rings that are not exactly circular in shape. Also, the process of marking the "mass

point" stations with reflectorized paint was a difficult one to control, resulting in "mass point" marks which were not equidistant from each other, and had variations in "length" (measured in the circumferential direction). Ideally, the "length" of the "mass point" marks should be in the same proportion as the "width" of the marks (measured in the radial direction) which is determined by the thickness of the ring. However, it should be noted that although the "mass points" on the ring were not equidistant and did not form an exact circle, they did represent the initial condition of the ring. The TEJ-JET program is capable of treating the initial conditions as represented, as it considers only the changes occurring from one instant of time to the other, and is valid also for a "grotesquely distorted" ring.

Also falling into this category would be the case of an improperly marked background reference point pattern. The subsequent computer analysis works on the assumption that the reference point positions are known accurately, and bases an inertial reference frame on the set of reference points; it also computes variations in magnification factors in different orientations of the image. Hence, any inaccuracies in the positioning of the reference points on the background plate will have an adverse effect on the reliability of the inertial frame of reference, and may also introduce incorrect magnification factors to the containment ring "mass point" positions. However, it should again be noted that this type of an error would be a constant error throughout the interaction time interval, and would have no effect on the data scatter discussed below.

4.3 Film Reading and Resolution Uncertainties

A major difficulty with the experimentally-obtained data has been the presence of scatter in the data on the position coordinates of the ring "mass points". This scatter was present

in a spatial sense in each individual picture taken at a specific instant of time during the ring-blade interaction, and was also present in the time domain, when the sequence of consecutive pictures obtained from the high-speed motion picture film was considered. In the spatial domain, the data scatter manifested itself as a discrepancy from the anticipated smooth curvilinear shape of the ring, were it the initial "circular" shape or the subsequent deformed shape. In the time domain, the data scatter manifested itself as a discrepancy from the anticipated smooth trajectory of individual points on the ring, or the expected stationary position of the reference points. The time-wise data scatter was also present in the center-of-gravity locus of the attacked ring, which represented the average position of all 72 "mass point" stations of the ring. Averaging the position components from 72 points, which in themselves may have scatter in the space domain, should average out the random errors contributed from the individual points. The scatter present in the center-of-gravity locus of the ring was hence attributed to difficulties in determining an "inertial reference frame" based on the background reference points, the position components of which were also individually subject to the spatial scatter described earlier for the ring "mass point" stations.

The random errors that were inherent in the systems employed were difficult to reduce further in magnitude. They stemmed from the fact that the camera, electronic flash, and film employed were functioning near their design limits and little room for improvement was available. Thus, the camera was operated near its maximum framing rate, and the electronic flash peak output was used to expose the medium high-speed film. Uniformity of exposure was difficult to obtain. The resulting pictures, when projected magnified on the film reader screen were grainy in nature, and the operator was confronted with centering the cross-hairs on clusters of the film grains of varying

density. A distinct outline of the individual marks, be they the reference points or the ring "mass points" or the blade reference bands, was not present. The ground glass on which the picture was rear-projected also added its share of grain. In addition, as the blade contacted the ring and scraped against it, the neighboring marks were clouded from a clear view by matter generated as a result of the metal-to-metal scraping. Hence the reliability of the data for the area of interest at or near the point of impact suffered. Also, the film reader carriage position (with the Cartesian coordinates shown as a digital readout) was difficult to modulate; occasionally the position coordinates changed in increments of two microns (skipping the intermediate value), the x-coordinate positioning knob freewheeled frequently followed by sudden engagement and an unexpected jump of a few microns, thus requiring a reversal in the positioning knob rotation with its attendant lag. Hence, an uncertainty of 2 or 3 microns was conceded as being "unavoidable" with the present photographic reading equipment.

To reduce the magnitude of the random errors, an averaging process was employed. After reading the coordinates of the full set of points in each picture, the process was repeated four times. Hence, four readings were available for each point, and the data quality could be judged by the approximate repeatability (or rare lack of repeatability) of the position coordinates obtained. In the subsequent analysis, the screened data, still showing random scatter, was improved by the use of analytic smoothing techniques. Subsection 4.5 discusses the methods employed to smooth the position data.

4.4 Optical Distortion Effects

Falling into this category would be the aggregate of the optical distortions contributed by the many stages of optical systems involved in exposing the film with the sequence of ring-blade interaction events, developing it, and then projecting it through the film reader equipment to obtain the numerical position data.

The optical distortion effects were believed to be variable during the test, or to have affected different parts of the exposed film to varying degrees. The variable distortion effects would of course be superposed on any optical distortion that might have been constant for the duration of the test.

The sources of possible optical distortion, some having effects constant throughout the interaction period and some contributing variable effects, may be identified as the following: (a) misalignment of or a distorted image reflection by the mirror in the spin chamber which deflects the camera's horizontal view to a vertical view of the test set-up; (b) distortion through the glass observation port in front of the camera; (c) distortions introduced by the many sets of lenses and mirrors within the camera system, particularly any wobble or vibration of the rotating mirror or film-carrying drum; (d) variations in film dimensional stability during exposure, developing, drying, and handling procedures; and (e) misalignment or distortions attributable to the film-sandwiching glass, lenses and mirrors, and the ground-glass projection screen of the film reader.

Rather than attempt to track down the individual errors and to introduce corrections or compensations at each level, the approach of obtaining the best possible image with the existing system under controlled conditions and then using a corrective transformation based on the known gridwork of background reference points was used. Thus, in the object plane the background reference points were known to be in specific locations. The Cartesian coordinates obtained through the film reader for these same reference points, magnified by an average magnification factor, formed an image which was not coincident with the actual pattern. The image showed distortions in both the radial and circumferential directions of the reference point patterns.

An analytical method of transforming the image plane reference points to the object plane reference positions was developed. The transformation function was selected to apply to locations intermediate to the reference points as well. Hence, the image plane ring "mass point" stations were also transformed to "optically corrected" inertial space positions by using the same transformation. The transformation function was recomputed for each individual picture. Thus the image plane reference point pattern in each picture governed the transformation to be applied for the correction of optical distortion effects. It should be noted then, that heavy reliance was given to the reference point positions as read, which in themselves were subject to the random errors associated with reading position components on the film reader.

4.5 Data Smoothing Techniques

The position data for the containment ring, obtained through experiments carried out with due care and careful controls, and subsequently analyzed and corrected for possible optical distortion, were still subject to random scatter. Since the solution process in the TEJ-JET concept uses the second derivatives of the position loci, any variation of the position loci from a smooth curvilinear shape will result in wild fluctuations of the approximated derivatives.

In view of the fact that there was a limit to which one could reduce the random experimental errors associated with locating the ill-outlined points on the projected images of the interaction events, the screened and optically-corrected data were subjected to analytical smoothing techniques. The methods found to be reliable and applicable for this analysis were: (a) spatial smoothing of the ring "mass point" position data by Fourier series representation and (b) timewise smoothing of the data points by Gram polynomial representation.

Thus, for a ring which was approximately circular in shape initially and underwent distortions which gave it an oblateness and a "localized cusp" at the zone of impact, the sum of an adequate number of terms (or harmonics) in the Fourier series is capable of representing the smoothed shape of the ring at each instant of time when a picture is available. The full Fourier sine and cosine series was employed, and the magnitude of the coefficient which multiplied each term determined the extent of the participation contributed by that term to the total. Thus, for the earlier part of the interaction where the ring did not develop the "local cusping", the higher-order Fourier harmonics had small coefficients and hence contributed little to the shape determination. With advancing time, the higher harmonics came into play as the ring shape was distorted further. Therefore, in the time domain, the variation of the magnitude of each individual Fourier coefficient determined the time history of the deflected ring shape. Again, since the Fourier coefficients were based on the shape of the ring at each instant of time and relied on position data subject to random scatter, the time histories of the individual Fourier coefficients fluctuated, although on a reduced scale because of the averaging effect of 72 "mass point" positions. The Fourier coefficients needed smoothing in the time domain; this smoothing was carried out by the Gram polynomial smoothing technique.

The Gram polynomials (Ref. 18) are orthogonal under summation, and an adequate number of polynomials can approximate the jagged curve represented by individual data points with a smooth curvilinear shape. The analytic representation of this curvilinear shape, of course, easily lends itself to the computation of time derivatives. Section 5 details the analytical smoothing techniques employed.

Due care should be taken in selecting the number of terms employed both for the spatial and time smoothing of the experimental data points. If only a few terms are used in the Fourier series, one may lose the definition of the "localized cusp" at the region of the ring impacted by the blade. If too many terms are used in the Fourier series, one may end up with a ring shape that follows very closely the scattered experimental position data. Thus, an adequate balance between "smoothing" of the points and "fitting" the analytic curve to the points should be determined. The same argument applies to the time domain smoothing by Gram polynomials. Employing only a few terms could smooth out rapid changes in the shape of the time history curves and blot from knowledge the existence of rapid accelerations, whereas employing too many terms would tend to fit all of the random fluctuations and generate incorrect acceleration estimates. Again, a balance between "smoothing" and "fitting" should be sought. Section 6 presents some results and discusses the criteria on which the analyst can make a judgment.

SECTION 5

SUBPROGRAMS FOR ANALYSIS AND REDUCTION OF DATA

5.1 General Requirements

To assist in the analysis and reduction process of preparing the experimental fragment interaction data for use in the TEJ-JET program, utility programs were developed. Some of these subprograms are necessary tools used in the step-by-step data reduction procedure, while others are employed as aids to display the resultant data in convenient form for quick analysis and evaluation. Figure 3 shows a chart identifying the data reduction and analysis paths. The series of subprograms used in the steps leading to the TEJJER subprogram shown in Fig. 3 falls under the first category of being necessary tools in the data reduction process and are discussed in this section. A future report will document the complete TEJ-JET program.

As discussed in the preceding section, the experimental data were subject to the cumulative effect of many sources of unavoidable errors inherent in the limitations of the test equipment, techniques, and initial data generation process. Hence, the need for evaluating the experimental data to determine the extent of the uncertainties and errors and to compensate for the shortcomings was indicated. This evaluation and correction process was carried out by means of accepted analytical techniques while exercising different options or criteria to balance the analysis or evaluation between the limits of stringency and practicality. In Subsection 5.2, the functions served by the subprograms used as utility tools are described.

5.2 Functions of the Subprograms

The position-versus-time history of the containment ring subjected to single-blade impact was available as a set of

position coordinates for each individual ring "mass point" station at each time "instant" recorded on the high-speed photo film strip. A set of four readings of the position coordinates was obtained for each point in each picture by reading the sequence of point positions in four successive passes with the film reader. This set of position history data represented the "raw data" to be analyzed and evaluated.

5.2.1 Subprogram ANALYZ

The intent of obtaining a set of four repeated readings of the same point was to compare the repeatability of reading the position coordinates within a certain tolerance, to identify the occasional data that exhibited a gross error, and to use the screened data in obtaining an averaged value more representative of the point position when "magnified" to actual size. This function was served by Subprogram ANALYZ.

Subprogram ANALYZ accepts the "raw experimental data" -- representing the set of four separate readings in each picture for the reference points, the ring "mass point" stations, and the blade reference marks -- with the x,y position coordinates given in microns in the film plane. The four values for the individual components of the coordinates are then compared to check whether they all fall within a specified tolerance. A built-in "filter" eliminates from consideration the occasional reading which may fall outside the tolerance, and computes an average position coordinate based on the remaining "valid" position data. The subprogram identifies the sets of position data that show difficulties, with appropriate symbols in the output; the judgment of the analyst on the validity of the resulting average may then be exercised. Additional screening decisions are also used in the process but are too elaborate to merit detailed discussion in this report.

Having thus eliminated the gross errors and improved the position data by the averaging process, ANALYZ then computes

an "average magnification factor" based on the position components of the background reference points in the film plane (in microns) and the known positions of the reference points on the actual background plate (in inches). In this "average magnification factor" no attempt is made to identify possible variations of the magnification factor in different directions or regions in the film plane.* Further, an inertial reference frame is established based on the reference points. The origin of the inertial reference frame is located at the point coincident with the "center of gravity" of equal masses imagined to be positioned at the reference points. The orientation of the inertial reference frame is based on the directions of the principal axes of these equal masses imagined to be positioned at the reference points.

Based on the average magnification factor, the average position components of all the points are cast into the inertial reference frame and computed as position coordinates in the actual object plane (in inches). The resulting "averaged position data" are presented as printed output and also keypunched in the proper format for use in the subsequent analysis.

5.2.2 Subprogram CORECT

Analysis of the averaged position data, cast in the inertial reference frame and adjusted for magnification to actual size, indicated the presence of aberrations attributable to possible optical distortions present in the experimental equipment. The fact that the averaged position data for the background reference points did not coincide with the actual known reference point locations laid the basis for an investigation of optical distortion effects. It was determined that the application of a single average magnification factor at all points of the image plane and for any orientation fell short

*This matter is taken into account later.

of representing the (slight) variations in magnification that existed and that distorted the image. The distortions were such that the actual circular and radial pattern of the reference points "assumed an oblate shape", and the angular separation of the radial lines varied in different quadrants of the image. Hence, a method of compensating for the optical distortion was developed to correct the data such that the reference point positions would coincide with the actual locations and all intermediate positions would also be adjusted by the proper interpolation. This function was served by Subprogram CORECT.

Subprogram CORECT accepts the "averaged data" -- representing the averaged data of four readings after screening for the elimination of gross errors -- which are cast in an inertial reference frame and are adjusted to actual size. The position coordinates of the background reference points and the actual locations of the reference points are then employed in a solution process to determine the proper correction factors.

The correct value of a position component can be approximated by a polynomial representation of the position components in the image plane. Thus, if, for example, 21 of the 24 reference point positions were available in the image plane, one could cast the quations in the following complete quintic polynomial form since a <u>complete</u>[+] quintic polynomial consists of 21 terms:

$$
\begin{aligned}
R_x = \; & \alpha_1 \\
& + \alpha_2 x + \alpha_3 y \\
& + \alpha_4 x^2 \; \alpha_5 xy + \alpha_6 y^2 \\
& + \alpha_7 x^3 + \alpha_8 x^2 y + \alpha_9 xy^2 + \alpha_{10} y^3 \\
& + \alpha_{11} x^4 + \alpha_{12} x^3 y + \alpha_{13} x^2 y^2 + \alpha_{14} xy^3 + \alpha_{15} y^4 \\
& + \alpha_{16} x^5 + \alpha_{17} x^4 y + \alpha_{18} x^3 y^2 + \alpha_{19} x^2 y^3 + \alpha_{20} xy^4 + \alpha_{21} y^5
\end{aligned}
\qquad (5.1a)
$$

and

[+]Interpolation error is minimized when <u>complete</u> polynomials are used.

$$
\begin{aligned}
R_y = \quad & \beta_1 \\
& + \beta_2 x + \beta_3 y \\
& + \beta_4 x^2 + \beta_5 xy + \beta_6 y^2 \\
& + \beta_7 x^3 + \beta_8 x^2 y + \beta_9 x y^2 + \beta_{10} y^3 \\
& + \beta_{11} x^4 + \beta_{12} x^3 y + \beta_{13} x^2 y^2 + \beta_{14} x y^3 + \beta_{15} y^4 \\
& + \beta_{16} x^5 + \beta_{17} x^4 y + \beta_{18} x^3 y^2 + \beta_{19} x^2 y^3 + \beta_{20} x y^4 + \beta_{21} y^5
\end{aligned} \tag{5.1b}
$$

where R_x and R_y are the correct x,y components of a reference point, respectively, and the α's and β's represent appropriate constants. The x,y terms in the polynomials are the "averaged data" reference point position components obtained from the image plane.

The above equations hold true for all of the reference points with the associated x,y position components. Thus, one can list the full set of equations and express them in matrix form:

$$\{R_x\} = [P] \{\alpha\} \tag{5.2a}$$

$$\{R_y\} = [P] \{\beta\} \tag{5.2b}$$

where $\{R_x\}$ and $\{R_y\}$ are column matrices representing the correct position components of the reference points:

$$\{R_x\} = \begin{Bmatrix} R_x^{(1)} \\ R_x^{(2)} \\ \cdot \\ \cdot \\ \cdot \\ R_x^{(21)} \end{Bmatrix} \qquad \{R_y\} = \begin{Bmatrix} R_y^{(1)} \\ R_y^{(2)} \\ \cdot \\ \cdot \\ \cdot \\ R_y^{(21)} \end{Bmatrix} \tag{5.3}$$

also $\{\alpha\}$ and $\{\beta\}$ are column matrices representing the constant terms multiplying the elements in the polynomial expression:

$$\{\alpha\} = \begin{Bmatrix} \alpha_1 \\ \alpha_2 \\ \cdot \\ \cdot \\ \alpha_{21} \end{Bmatrix} \qquad \{\beta\} = \begin{Bmatrix} \beta_1 \\ \beta_2 \\ \cdot \\ \cdot \\ \beta_{21} \end{Bmatrix} \tag{5.4}$$

and the matrix $[P]$ has the elements of the polynomial expression for each reference point, thus comprising a 21x21 square matrix:

$$[P] = \begin{bmatrix} 1 & x_1 & y_1 & x_1^2 & x_1y_1 & y_1^2 & x_1^3 & \cdot & \cdot & \cdot & y_1^5 \\ 1 & x_2 & y_2 & x_2^2 & x_2y_2 & \cdot & \cdot & \cdot & \cdot & \cdot & y_2^5 \\ \cdot & \cdot & \cdot & \cdot & \cdot & \cdot & \cdot & \cdot & \cdot & \cdot & \cdot \\ \cdot & \cdot & \cdot & \cdot & \cdot & \cdot & \cdot & \cdot & \cdot & \cdot & \cdot \\ 1 & x_{21} & y_{21} & x_{21}^2 & \cdot & \cdot & \cdot & \cdot & \cdot & \cdot & y_{21}^5 \end{bmatrix} \tag{5.5}$$

All the elements of the $[P]$ matrix can be computed from the "averaged data" position components of the reference points. The correct position components $\{R_x\}$ and $\{R_y\}$ of the reference points are also known. Hence, with the proper matrix solution techniques, one can solve for the constants $\{\alpha\}$ and $\{\beta\}$.

Having determined $\{\alpha\}$ and $\{\beta\}$, one may then calculate the "correct position" R_x and R_y for each new point with coordinates x and y, according to the polynomial representations.

It was established, however, that the solution for the quintic polynomial with 21 unknowns gave (as must be the case mathematically) the exact values at the reference point positions, but developed extreme oscillations in regions intermediate to the reference points. The use of lower order polynomials (with smaller numbers of unknowns) but using all 21

equations equally weighted gave slightly poorer fit at the reference points but much improved smooth interpolation between the reference points, where the ring "mass point" positions were. Applying a cubic polynomial fitting for example, gave plausible corrected ring "mass point" positions. This implies that the [P] matrix may be a non-square matrix, with 10 columns for a cubic polynomial expression, and 21 rows. The solution process employed is described in Ref. 16.

Subprogram CORECT thus provides a set of "corrected data" free of optical distortion. The data are provided as printed output and also keypunched on cards with the appropriate format for the subsequent analysis.

5.2.3 Subprogram SMOOTR

The set of "corrected data" provided as the output of the preceding utility subprograms represents position data that have been screened to eliminate obvious errors in reading position coordinates, then averaged on the basis of the remaining valid data readings, and subsequently corrected for magnification and optical distortion effects. However, the position data still suffer from random experimental errors associated with the reading of (a) the reference points and (b) the ring position data from a projected image of the high-speed film. These errors are admittedly small in magnitude but are of importance in an analysis which requires the availability of time derivatives based on the displacements provided by the position data. A smooth position-versus-time locus could of course be differentiated conveniently and give reasonable velocity and acceleration data, whereas a jagged position-versus-time locus would result in rapidly changing velocity and acceleration with large magnitudes. Smoothing the avail-

able "corrected data" by employing accepted analytical smoothing techniques would eliminate the random scatter of data points and render the data amenable for differentiation to obtain plausible velocity and acceleration estimates. It should be noted, however, that a low order of fitting the data points in an effort to eliminate random scatter could result in smoothing out an important change in curvature of the position locus and mask from knowledge the associated velocity and acceleration changes. In the other extreme, a tightly-fitted smooth curve would tend to approximate the position of all data points and reflect the attendant superfluous changes in position locus curvature while following the scattered data points closely. Hence, an adequate and sufficient amount of smoothing should be introduced to eliminate the random experimental errors from the "corrected data". This function is served by Subprogram SMOOTR.

Subprogram SMOOTR accepts the "corrected data" -- representing the optically-corrected averaged position data -- and smooths the data both spatially within each picture and timewise in the sequence of pictures. The spatial smoothing of the ring "mass point" position data in each individual picture (or associated instant of time) is achieved by employing Fourier series to represent the harmonic components of the ring shape. An adequate number of terms, determined by the analyst, are used in the summation of both the sine and cosine series. Thus

$$F_V = A_{V_o} + \sum_{n=1}^{N} A_{V_n} \cos n\theta + B_{V_n} \sin n\theta \qquad (5.6)$$

$$F_W = A_{W_o} + \sum_{n=1}^{N} A_{W_n} \cos n\theta + B_{W_n} \sin n\theta \qquad (5.7)$$

where F_V and F_W are the Fourier representation of the two Cartesian components of the ring "mass point" position data,

θ is the angular position of the "mass point" in the inertial reference frame, all of the A_v, B_v, A_w, B_w, terms are the Fourier coefficients multiplying the cosine and sine series, and N is the total number of terms in the Fourier series.

For a perfectly circular ring, the coefficients A_{v_o} and A_{w_o} are the horizontal and vertical position components, respectively, locating the ring's center of gravity in the inertial reference frame; the coefficients A_{v_1} and B_{w_1} are equal to the ring radius and hence $F_v = A_{v_1}\cos\theta$ and $F_w = B_{w_1}\sin\theta$ represent the circular shape of the ring about the center of gravity position A_{v_o}, A_{w_o}. All other coefficients are equal to zero and the associated Fourier series terms contribute nothing to the ring shape.

As the ring deforms under impact, the time-history of the coefficients of the zeroth harmonic, A_{v_o} and A_{w_o}, will represent the rigid body motion (center-of-gravity locus) of the ring; changes in the magnitude of the coefficients of the first harmonic, A_{v_1} and B_{w_1}, will represent the expansion or contraction of the circular shape of the ring (the breathing mode); non-zero values for the coefficients of the second Fourier harmonic, A_{v_2}, B_{v_2}, A_{w_2}, and B_{w_2}, will represent the oblateness of the ring in orientations determined by the relative magnitudes of the constants; and higher order harmonics will further contribute to a fuller description of the distorted shape. It should again be noted that a large number of Fourier harmonics will follow the scattered position data too closely and accept superfluous distortions as valid data, whereas a small number of Fourier harmonics will be inadequate as an important local distortion may be smoothed out and unintentionally discarded (lost information results). The analyst has to determine an appropriate compromise between the two limits. The criteria on which a decision can be based are explained in Section 6.

The smoothing in space then results in the determination of the magnitudes of the Fourier coefficients multiplying the terms in the Fourier series. As the interaction time advances, the magnitudes of the coefficients will change to reflect the distorting shape of the ring. The coefficients for the higher order harmonics in particular will exhibit increases in their magnitude with increasing distortion. Hence, if one were to plot the values for each coefficient against the associated time, one would obtain curves representing the variation in time of the constants. These curves may also be subject to some experimental data scatter for the same reasons that the stationary background reference points show scatter in the time domain. An incorrectly-read position of a not-well-outlined reference point may inadvertently affect the ring position data.

The smoothing in time is carried out by using Gram polynomials[+] (Ref. 18) to smooth the locus described by each Fourier coefficient in the series. As a result of this smoothing, the distortion of the ring will progress smoothly from one instant of time (picture record on the high-speed motion picture film) to the next.

Gram polynomials are used to calculate a smooth curve approximation to a set of discrete data as follows:

$$f(s) \cong \sum_{r=0}^{n} a_r p_r(s,N) = y(s) \tag{5.8}$$

where f(s) are the discrete points to be smoothed

p_r is the rth Gram polynomial defined below.

a_r is the rth Gram coefficient, determined such that f(s) is approximated in a least-squared error sense.

[+]Gram polynomials are appropriate for the present discrete-data application since they are orthogonal under summation (the Legendre polynomial counterpart for continuous data, as discussed for example in Ref. 5, is orthogonal under integration).

N is one less than the number of data points.

s is the abscissa variable (s = 0, 1, 2, 3, ...N)

and n is one less than the total number of coefficients used to approximate f(s), where $n \leq N$.

The general equation for the rth Gram orthogonal polynomial is:

$$p_r(s,N) = C_{rN}\left[1-\frac{r(r+1)}{(1!)^2}\frac{s}{N}+\frac{(r-1)r(r+1)(r+2)}{(2!)^2}\frac{s(s-1)}{N(N-1)}\right. \tag{5.9}$$

$$\left.-\frac{(r-2)(r-1)r(r+1)(r+2)(r+3)}{(3!)^2}\frac{s(s-1)(s-2)}{N(N-1)(N-2)}+\text{etc.}\right]$$

where C_{rN} is an arbitrary constant (see page 289 of Ref. 18).

If one makes use of an odd number of points, so that N is even, then one can define

$$M = N/2$$

and

$$s = M + t \text{ (see sketch below)}$$

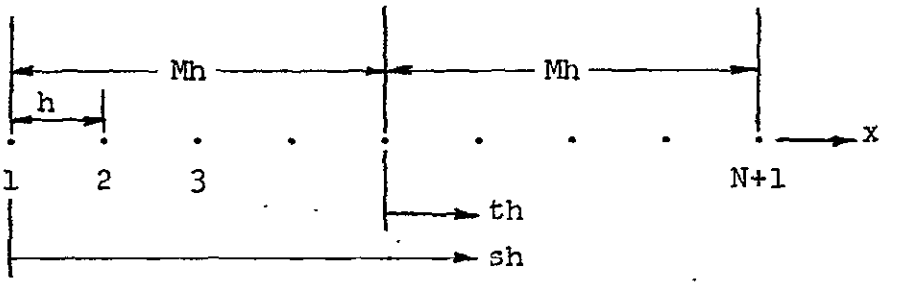

Also, choose

$$C_{rN} = (-1)^r \tag{5.10}$$

When these changes in variables are accomplished, the first 6 polynomials can be written as follows:

$$p_0(t,2M) = 1$$

$$p_1(t,2M) = t/M$$

$$p_2(t,2M) = \frac{3t^2 - M(M+1)}{M(2M-1)}$$

$$p_3(t,2M) = \frac{5t^3 - (3M^2+3M-1)t}{M(M-1)(2M-1)} \qquad (5.11)$$

$$p_4(t,2M) = \frac{35t^4 - 5(6M^2+6M-5)t^2 + 3M(M^2-1)(M+2)}{2M(M-1)(2M-1)(2M-3)}$$

$$p_5(t,2M) = \frac{63t^5 - 35(2M^2+2M-3)t^3 + (15M^4+30M^3-35M^2-50M+12)t}{2M(M-1)(M-2)(2M-1)(2M-3)}$$

and the approximation for the discrete points becomes:

$$f(t) \cong \sum_{r=0}^{n} a_r p_r(t,2M) = y(t) \qquad (5.12)$$

where

$$t = -M,\ -M+1,\ .\ .\ .,\ 0,\ .\ .\ .,\ M-1,\ M \qquad (5.12a)$$

Higher-order polynomials can be obtained from the following recursion formula (Ref. 19):

$$p_{r+1}(t,2M) = \frac{2(2r+1)}{(r+1)(2M-r)}\, tp_r(t) - \frac{r(2M+r+1)}{(r+1)(2M-r)}\, p_{r-1}(t) \qquad (5.13)$$

These polynomials posess the following orthogonality property:

$$\sum_{t=-M}^{M} p_q(t,2M)\, p_r(t,2M) = \delta_{qr}\gamma_r(2M) \qquad (5.14)$$

where

δ_{qr} is the Kronecker delta, and

$$\gamma_r(2M) = \frac{1}{2r+1} \frac{(2M+r+1)^{(r+1)}}{(2M)^{(r)}} \qquad (5.15)$$

and the factorial nth power of s is defined to be (where n is a positive integer)

$$(s)^{(n)} = s(s-1)(s-2) - - - - (s-n+1) \cong \frac{s!}{(s-n)!} \qquad (5.16)$$

where $(s)^{(o)} = 1$.

The a_r's are independent and can be calculated as follows:

$$a_r(2M) = \frac{1}{\gamma_r(2M)} \sum_{t=-M}^{M} f(t)\, p_r(t,2M) \qquad (5.17)$$

The data points to be smoothed are f(t). Note that the Gram polynomials are orthogonal under properly-weighted summation.

Thus, the Fourier coefficients -- the discrete data points f(t) to be smoothed -- undergo the Gram polynomial smoothing in time. Program SMOOTR then gives as punched output the set of coefficients of the Gram polynomials, a_r, needed to smooth the Fourier coefficients, A_V, B_V, A_W, B_W. This punched output is in the proper format to be used as part of the input to the TEJJER program, which reconstructs the smoothed Fourier coefficients and calculates the smoothed position data based on the Fourier harmonic content. The printed output of subprogram SMOOTR also shows the initial position data, the initial Fourier coefficients, and the subsequently smoothed Fourier coefficients for preliminary checks on the adequacy of the smoothing achieved.

5.2.4 Subprograms CGLOX, PREADD, and FORCER

This group of subprograms provides a second branch (parallel to subprogram SMOOTR described in the previous subsection) leading into a second input into the TEJJER program. Whereas subprogram SMOOTR provides a means to calculate space and time smoothed individual ring "mass point" position data for the calculation of interaction forces, the group of subprograms CGLOX, PREADD, and FORCER provides an estimate of the total force acting on the ring based on the knowledge of the center-of-gravity locus and the rotation, θ, of the ring. The three subprograms are an integral set, but are not combined within one program because of the need for analyst judgment and action at the intermediate-answer stages. At the end of each subprogram, the results are to be assessed and some options are to be exercised prior to input into the following subprogram for analysis.

Subprogram CGLOX accepts the "corrected data" in representing the optically-corrected averaged position data -- as does the previously-described subprogram SMOOTR. The individual ring "mass point" position data are then used to obtain the Cartesian coordinates of the ring's center-of-gravity and the angular orientation of the ring in the inertial reference frame for each picture (instant of time). The sequence of pictures thus provides the ring center-of-gravity locus and angular rotation versus time. Any accelerated motion of the center-of-gravity or rotation of the initially-stationary ring would, of course, be caused by external forces, such as those generated by the impact of the blade fragment. A force applied at an oblique angle to the ring's circumference would cause the rotation as well as the translation of the containment ring, in addition to localized bending. The subprogram output in printed and keypunched form gives the Cartesian components of the center-of-gravity as well as the angular rotation as discrete data for the sequence of pictures.

Since the ring is stationary prior to impact, the position of the center of gravity and ring orientation during that time are stationary, and one may pre-add a certain number of data points to establish the pre-impact stationary loci, using the same values as those provided by the first picture. It should of course be ascertained that the first picture does indeed record a pre-impact condition. Subprogram PREADD is a simple utility program which pre-adds the specified number of points and prepares the keypunched input data cards in the proper format for subsequent use.

The data at this point represent the center-of-gravity locus and the rotation of the containment ring. Plotted versus time, the data again exhibit the scatter due to experimental uncertainties in reading individual-point positions, including the reference points, from high-speed motion picture frames. Hence, the smoothing of the discrete data points in the time domain becomes necessary, prior to obtaining the center-of-gravity accelerations and the angular accelerations on which an estimation of the total forces is based. Subprogram FORCER serves this function. The time smoothing is accomplished through Gram polynomial approximations of the discrete data point locations similar to the technique described for subprogram SMOOTR in Subsection 5.2.3. The points pre-added to the center-of-gravity locus and angular rotation history establish data to represent the known stationary nature of the ring prior to impact. Because the Gram polynomial approximation degenerates near the two ends of the curve being fitted, the pre-added points guarantee that the unreliable part of the smoothing technique occurs at times prior to the time of interest (the initiation of the impact). The availability of data points from pictures well after the completion of the impact interaction provides the necessary additional points at the other end of the curve to "absorb" the uncertain region of smoothing beyond the time of interest (the termination of the interaction).

Subprogram FORCER thus accepts the center-of-gravity locus and ring rotation data, and smooths the data in time by employing a specified number of Gram polynomials for the approximation. The contributions of each polynomial are printed out, as well as the sum total of all polynomials fitting the curve, in addition to the coefficients multiplying the polynomials. The analyst thus has the option of checking the results to determine the adequacy of the smoothing. Having generated the polynomials fitting the discrete data, subprogram FORCER computes the first and second derivatives of the curves and obtains the total accelerations which the containment ring undergoes. With the knowledge of the ring mass and moment of inertia, the total force history is calculated and printed out for each option of Gram-polynomial smoothing. The total computed force is highly dependent on the amount of smoothing employed, and the analyst should judge which result gives the best plausible total force estimate as a function of time. Since the actual externally-applied forces experienced by the ring vary both timewise and in spacewise distribution along the ring when the impact sequence occurs, the analyst must apply some judgment or estimation method if he wishes to deduce this type of force-distribution time history data from the present total force information. In this process he can make use of his knowledge of roughly where and when the fragment impacts occur along the ring as can be seen from the sequence of motion-picture photographs.

In Section 6 the criteria used to judge the adequacy of the smoothing, along with the presentation of results are discussed. This information then becomes the second branch of the input in the TEJJER program, to be used in addition to the smoothed individual "mass point" position data provided by subprogram SMOOTR. A Kalman filter within TEJJER provides the means to weight the data according to associated levels of reliability prior to using the data in the calculation of estimated "optimum external forces" acting on the containment ring.

SECTION 6

APPLICATION OF THE SUBPROGRAMS

6.1 Motivation and Objectives

In order to examine the theoretical feasibility of the TEJ-JET scheme for deducing externally-applied transient forces from detailed transient structural motion/deformation data, the JET2 computer code was employed to predict the transient large elastic-plastic deformation response of an initially-circular ring subjected to a specified distribution and time history of externally-applied forces. This "correct" structural response information was then "contaminated" to simulate errors which inevitably would be present in experimental measurements of this structural response behavior; this contamination was achieved by perturbing the correct structural response information by random numbers having a zero mean value but with various levels of probable error. This contaminated information was then subjected to the TEJ-JET analysis scheme, and the resulting predictions of the distribution and time history of the externally-applied forces were in very good agreement with the specified externally-applied forces (Ref. 5).

Subsequently, structural response measurements conducted at the NAPTC for single-blade impact against containment rings (NAPTC Tests 88 and 91) were analyzed (Ref. 5). These data were studied to ascertain the kinds and magnitudes of the errors contained in these data (as in all experimental data); also, the likely sources of the errors were identified. Because of the error level present, the TEJ-JET predictions of the associated external forces were of low reliability.

After having devised (a) improved techniques to minimize experimental measurement errors and (b) improved procedures of analysis and error compensation, NAPTC Test 165 for impact/in-

teraction of a single blade from a T58 turbine rotor against a containment ring was conducted. The motion picture data were read as described in Section 4; however, study of these data showed that repeated readings from the same picture showed some inconsistencies. Therefore, a second complete reading of this film was carried out with great care and careful cross-checking. The remainder of Section 6 is devoted to discussing the subsequent analysis of this "second reading" of the position data for NAPTC Test 165.

6.2 Error Magnitudes in the Experimental Data

The position components of each data point on the film which recorded the blade/ring interaction were read four times in each picture frame. The four repeated readings showed rare irregulatities in repeatability when the results were checked by employing Subprogram ANALYZ with a tolerance or "test distance" of 12 microns in the film plane (approximately 0.045 in. in the object plane). Repeatability in most instances was well within half of that tolerance, or approximately 0.02 in. in the object plane. However, it should be noted that this concerns the reading of the same point in one picture frame. Variations in film grain, distortion, lighting, and other causes may lead the analyst to select a somewhat different part of the same data mark on which to center the cross-hairs in subsequent picture frames. This possibility is shown graphically in Fig. 4, where the results obtained from pictures 1 and 2 are compared; both are for the pre-impact condition. Here, the four readings for each ring "mass point" position component have been averaged after the elimination of gross errors, via Subprogram ANALYZ. Since both pictures 1 and 2 are recorded prior to the moment of blade impact against the containment ring, the pictures should show a static ring; position components obtained from one should, ideally, match the other. Figure 4a depicts the differences in

the horizontal-position components, and Fig. 4b depicts the differences in the vertical-position components for "mass points" of pictures 1 and 2. Note that the error bandwith is approximately 0.04 in. and that the "averaged data" employed at this stage is prior to any corrections for optical distortion or any smoothing in time and space.

In addition, similar uncertainties in reading the reference marks produce errors in locating the reference frame, which in turn affect the location of all position coordinates referred to that plane. The presence of errors in reading the stationary reference mark positions from the high-speed motion pictures is shown in Fig. 5. The apparent variation of the position of reference points 1,2, and 3 (three points on a radial line) as a function of time (sequence of pictures) is shown in Fig. 5a for the horizontal component, and in Fig. 5b for the vertical component. The error bandwidth is again approximately 0.04 in. and the resultant uncertainty in the reference frame derived from such reference points definitely has a bearing on the ring position data*. This behavior is discussed further in Subsections 6.3-6.5.

6.3 Effects of Optical Distortion

The conversion factor employed in Subprogram ANALYZ to convert positions from the film plane to the object plane was a constant factor for each picture. The average radial distance of the reference points from the origin of the reference frame was compared versus the corresponding distance in the actual reference background plate in determining the average conversion factor. Closer scrutiny of the reference point positions obtained from a reading of the film with the application of the average conversion factor indicated that the

*The results presented in Figs. 4 and 5 are in the film reader axis system (subscript R). Results presented in subsequent figures are in the inertial frame derived from the reference grid (no subscript).

variation in the reference point positions was considerable, and was beyond any random effects. This is illustrated in Figs. 6a and 6b for the radial and circumferential components, respectively, of the set of reference points as seen in the first four pictures of the film*. Note that both radial distortion and circumferential distortion behave as essentially symmetric oscillations, with the circumferential distortion lagging 45° in phase compared with the radial distortion. This observation applies to all of the picture frames. The radial distortion thus "gives an elliptical shape" to the actual circular pattern of the reference points (and hence to the circular ring) while the circumferential distortion oscillates in a 1.5-deg amplitude about a minus 2.3-deg mean value+.

The analytical methods of correcting for the existing optical distortion, as described in Subsection 5.2.2, were subsequently employed to account for the variable magnification factors existing at different regions of the film plane. The optically-corrected reference point positions from picture number one are shown in Figs. 7a and 7b for the error magnitude in the radial component and in the circumferential direction, respectively*. Each figure presents the results of four polynomial-fitting solutions, based on the known position of the reference points in the actual object plane. The four results shown are for the linear, quadratic, cubic, and quartic polynomials. The quintic polynomial, employing all 21 terms of the expression to solve for the 21 unknowns, gave the exact solution for all of the reference point positions, as expected. However, as explained earlier in the analytic presentation, positions intermediate to the reference points showed extreme

*To aid the reader in visualizing how each ordinate quantity varies with the abscissa coordinate, curves have been faired through the data points.

+This θ = -2.3-degree location represents the orientation of the reference line passing through points 1,2,3,15,14, and 13 (see Fig. 1) with respect to the "principal axes" of the optically-distorted reference point array.

oscillations for the quintic-polynomial-solution case.

The adequacy of lower order polynomial fitting is shown in Fig. 8 where the horizontal and vertical components of the ring "mass point" positions are shown. The results obtained from the linear, quadratic, and cubic polynomial fitting are essentially the same, as shown in the plot, for the number of significant figures that can be identified at the scale shown. However, the quartic polynomial fit, not depicted in Fig. 8, gives results noticeably different from the plot shown. Were they plotted, they would show an oscillatory shape (albeit of small amplitude) superposed on the sinusoidal shape of the position components depicted. Figure 9 presents the same position data from a segment of the ring (the first ten "mass points") on an expanded scale. The original position components are shown as a basis for comparison against the linear, quadratic, cubic, and quartic polynomial fitting results. Note the similarity of results for the first three polynomial fitting solutions, but the deterioration in fitting the correct shape when the quartic polynomial fitting is employed. For the above reasons, the cubic polynomial fitting to correct for optical distortion was determined to be adequate, and further analysis was carried out on the data thus corrected.

It should again be stressed that the data corrected for optical distortion still include experimental errors associated with the reading of the reference point and ring "mass point" position data. Actually, incorrect reading of the position components of an ill-defined reference point would inadvertently affect the optical correction process. However, with information from 21 reference points employed, the chances of incorrect compensation for optical error are reduced considerably.

6.4 Spatial Smoothing of Ring Position Data

The optically-corrected ring position data, still subject to scatter due to experimental uncertainties, were smoothed analytically in space, as explained in Subsection 5.2.3.

Fourier sine and cosine series were employed to fit the experimental position data with smooth curves. The magnitudes of the Fourier coefficients determine the contribution each term brings to the total harmonic content of the smooth fit to the ring position data. As the ring/blade impact interaction time advances, the changing shape of the ring causes changes in the magnitudes of the Fourier coefficients, to reflect the varying harmonic content. In particular, with the local bending of the impacted ring, the higher order terms contribute more and more to the description of the ring shape. Thus, the magnitudes of the higher-order Fourier coefficients show an increase as time progresses.

The above effect is presented in Figs. 10a, 10b, and 10c where the coefficients of the first, second, and third Fourier harmonics are shown, respectively, as a function of time. The first harmonic, of course, describes the circular shape of the ring, and any expansion or contraction (the breathing mode) of the ring. Note that the presence of both sine and cosine contributions in either of the horizontal or vertical axis directions is due to the fact that the impact-induced cusp in the ring does not coincide with either the Y or Z axis. Hence, the varying values of the coefficients include the effects of ring rotation (thus changing the θ = 0-deg axis orientation) in addition to the breathing mode. The second harmonic describes the oblateness of the ring, as defined by the magnitude of the Fourier coefficients depicted in Fig. 10b. Here, the ring is originally shown to have negligible oblateness (magnitudes of the coefficients are nearly zero) but the degree of oblateness is shown to increase with the passing of time. Again, the orientation of the oblateness is determined by the relative magnitudes of the Fourier coefficients. The same observations of negligible initial contribution and increasing magnitudes of Fourier coefficients with advancing time hold true for the higher Fourier harmonics, similar to the

case for the third Fourier harmonic depicted in Fig. 10c, which contributes a tri-lobed component to the distorted shape of the Fourier series spatial smoothing. It should be noted that the maximum magnitudes of the coefficients tend to be smaller for the higher-order harmonics, indicating relatively smaller contributions from them to the general shape of the smoothed positions. One should also note that the figures show eight pre-added points, having the same values as the coefficients for the first picture, to establish the pre-impact stationary shape of the ring.

As a final observation, the reader's attention is drawn to the fact that the time history of each coefficient shows some scatter, so that the transition from one picture to the next one is not exactly smooth.

6.5 Timewise Smoothing of Ring Position Data

Following the spatial smoothing of the data points, the next task was the smoothing in the time domain. The position data expressed as a smooth function of time lend themselves to easier differentiation and give plausible results of velocity and acceleration estimates, as opposed to the differentiation of jagged position loci which would indicate rapidly changing velocities and accelerations. The timewise smoothing is accomplished through the use of Gram polynomials, as explained in Subsection 5.2.3. The magnitudes of the Gram coefficients determine the contribution of each Gram polynomial to the smoothing fit.

A representative result showing the magnitudes of the Gram coefficients employed to smooth the loci of the Fourier coefficients depicted in Fig. 10b for the second Fourier harmonic is shown in Fig. 11. The normalized magnitudes of the four coefficients are shown on a logarthmic scale, indicating the rapid decline in the order of magnitude for the higher-order

Gram coefficients. Similar results are obtained for the timewise smoothing of the coefficients for the other Fourier harmonics. It should be noted that no definite cutoff exists beyond which one may neglect including the higher-order Gram polynomials. The higher-order terms contribute smaller amounts to the total function, but are important to a degree in preserving the representative character of the position loci by approximating closely the data points. However, including too many higher-order terms tends to fit the scattered data points so closely that differentiation to obtain velocity and acceleration gives implausible results.

The sensitivity of the results to the timewise smoothing is best indicated by carrying through the analysis of the center-of-gravity locus and rotation of the impacted ring. Figure 12 shows the horizontal and vertical components of the center-of-gravity locus and the ring's rotation versus picture number. The cg is, of course, determined by averaging the positions of the 72 ring "mass points", and is also equivalent to the zeroth Fourier harmonic. However, despite this averaging based on a relatively large number of components, data scatter is still evident. Part of this is attributable to the uncertainties involved in the reference frame determination, based on the available reference point position data.

The magnitudes of the coefficients for the Gram polynomials needed to smooth the cg locus and ring rotation in time are depicted in Fig. 13 for the two Cartesian components and the ring-rotation component. Eight pre-impact points were pre-added to the cg locus, duplicating the position components of picture number one, to establish the stationary ring existing before the interaction.

The timewise smoothed cg locus and ring rotation is shown in Fig. 14 for the cases of (a) 5 and (b) 10 Gram polynomials[+]. Note that the 10 Gram polynomial case appears as an oscillation superposed on the 5 Gram polynomial case. The 6 through 9 Gram polynomial cases are not presented here to avoid crowding the figure;

[+] These pertain, respectively, to n = 4 and n = 9 in Eq. 5.8.

however, they each result in minor corrections to the center-of-gravity locus keeping in perspective the scale employed in the plots. The time derivatives of the cg locus, of course, show greater sensitivity, and will be discussed next.

6.6 Total Collision-Induced Forces Estimated from the CG Locus

As discussed in Subsection 5.2.4, an estimate of the total collision force imparted by the attacking blade fragment to the containment ring is made based on the acceleration history of the cg of the ring. The acceleration of the ring is gleaned from the timewise smoothed cg locus, as its second time derivative.

The force component imparted in the horizontal direction of the reference frame is shown in Fig. 15 for each individual Gram polynomial used in fitting the cg locus. Thus, the contribution of each term is shown individually to enable one to visualize the contribution which each additional term of the Gram polynomial introduces to the total force estimate.

Note that the third Gram polynomial term reduces to a constant upon differentiation twice, as evidenced by the constant value shown in Fig. 15. The fourth term introduces the linear variation, the fifth term introduces the quadratic variation, and so on. The divergence at the two extremities is as anticipated, and is limited to the intentionally pre-added pre-impact positions and the segment of time after the interaction time of interest in the analysis. The above results include the effect of the Gram polynomial coefficients as shown in Fig. 13, and hence the magnitude of the contribution of each term is governed by the magnitude of the coefficient.

Figures 16a and 16b show the time history of the horizontal and vertical components, respectively, of the estimated total force acting on the ring, as a function of the number of Gram polynomials employed for the smoothing. It is clear that the choice of the number of smoothing polynomials defines the shape of the cg locus, and hence the estimated force based on its second time derivative (acceleration). The lower numbers are inadequate to depict the forcing functions, whereas the higher numbers fit the scattered points closer than desirable and result in the estimation of erratic total forces.

A plausible estimate of the total force was selected to be a faired curve through the average of the curves labeled 7,8,9, and 10 in Fig. 16. The resulting estimated force history components in the Y and the Z direction are shown in Fig. 17. The time history of the estimated total force is consistent with the time history of the blade-to-ring impact location which is observed to commence in the fourth quadrant of the inertial reference frame system and to progress clockwise to the third quadrant. Thus the horizontal component starts as a force in the positive direction, then crosses over to a negative value in the third quadrant, whereas the vertical component is in the negative direction throughout --- as can be seen readily from Fig. 17 in conjunction with Fig. 18.

An examination of the sequence of motion pictures enables one to estimate the location of the zone of blade/ring impact as time progresses. This is shown in Fig. 18. At each time instant the total force depicted in Fig. 17 may be regarded as being distributed in some plausible fashion over the blade/ring impact zone. Accordingly, this provides one estimate of the distribution and time history of the blade/ring collision-interaction forces.

Although not discussed in this report*, a second estimate of the blade/ring collision-induced forces may be made by a TEJ-JET

*A future report will deal with this more complex matter.

analysis of the motion of the individual "mass points" of the ring, rather than of the ring's cg. This leads automatically to a determination of the magnitude and time history of the externally-applied forces acting upon each ring "mass point".

By means of a Kalman filter scheme in the TEJ-JET program, both of the above forcing function estimates are combined, while applying appropriate weighting factors for each, in order to obtain an "optimum estimate" of these externally-applied forces. These matters will be discussed appropriately and more fully in a future report.

SECTION 7

SUMMARY AND COMMENTS

The need for rational structural design methods to design structures for either containing or deflecting (into "harmless" regions) engine rotor fragments from aircraft jet engines is discussed. It is argued that efficiency and convenience considerations lead one to employ two-dimensional rather than shell and/or three-dimensional-solid structural analysis models at this time. Further, the judicious use of both theoretical analysis and experimental data on engine-rotor-fragment impact with selected structures is essential to achieve reliable and efficient designs for this complex problem since only a limited understanding of its many aspects currently exists.

Accordingly, restricting attention to fragment containment/deflector structures whose deformations are confined essentially to one plane (the plane of the structural ring), it was noted that already-validated methods for predicting the large-deflection elastic-plastic transient deformations of such structures are available; reliable and accurate predictions result provided that one has accurate knowledge of the externally-applied transient forces to which the structure is subjected. In the present context, these forces are the forces applied to the structural containment/deflector ring by the impacting fragment(s) during the impact and interaction process. A means for estimating these impact/interaction forces experienced by the "ring" is to conduct experiments in which (a) selected types of engine-rotor fragments are caused to impact "typical" rings and (b) careful measurements are made of the transient response and deformation of the impacted structure. This information is then used in a "backward-solution" of a JET structural response

computer code to obtain an estimate of the externally-applied forces which must have produced the experimentally-measured transient motion and deformations of the fragment-impacted ring; this procedure is termed the TEJ-JET process.

The theoretical feasibility of the TEJ-JET process was established earlier. The present report describes work in progress to assess whether or not this scheme is feasible in a practical sense when experimental transient deformation data of the limited precision and accuracy provided by currently-available techniques are employed.

In this report the experimental equipment and the techniques employed at the Naval Air Propulsion Test Center (NAPTC) for generating the needed data are described. Particular attention is given to identifying possible sources of error and uncertainties in obtaining the sought experimental data, since the success of the TEJ-JET process depends upon obtaining experimental transient structural motion and deformation data of high accuracy. Accordingly, discussed are the careful control of the experimental steps involved -- beginning with the equipment and the test arrangements -- to the generation of the high-speed motion picture film recording of the impact-response behavior, and culminating with the readout from each picture of the film of the coordinates (or position) of the deformed structure using a Nuclear Research Instruments Corp. optical film reader. In reading the film, the viewer must exercise his judgment in deciding where to position the reading cross-hairs to locate the coordinates of a given "spot" on the structure; repeated readings of a given spot will produce slightly different results and, thus, some data uncertainty is present from this source.

In addition to identifying possible sources of error in the generated transient position data of the structure (and of the fragments), analytical means are described to compensate

for (a) uncertainties in reading the "structural station" position data, (b) optical distortion effects (camera system, film shrinkage, optical reader, etc.), and (c) other random errors in the position data in both space and time. For the last of these items, data smoothing: (1) in space by means of Fourier series and (2) in time by means of Gram polynomials, is employed.

To illustrate these techniques, data from NAPTC Test 165 involving the impact of a single blade from a T58 engine turbine rotor against an aluminum containment ring are analyzed. These studies reveal the magnitudes of the errors* present in the experimental data and also show the effects of the analytical compensation and smoothing techniques employed to analyze the data. To date only one of the two "force extraction" branches of the breadboard TEJ-JET program has been followed through to completion to determine the impact/interaction forces -- this branch deals with analyzing the motion of the CG of the ring and deduces therefrom the total force which acts upon the ring as a function of time. At any instant, this total force is assumed to be distributed over a small region of the ring where the film records show the impact/interaction to be occurring. From this analysis branch, the estimated total force history is found to be plausible and physically consistent.

The second branch of the TEJ-JET process is designed to produce information on the components of the transient external force acting on each "mass point" of the structural ring. The exercising of this second branch on the (improved) NAPTC Test 165 data has not yet been carried to completion. Thus, the present report constitutes an interim progress report on the practical feasibility of the TEJ-JET method. This work, how-

*Improved techniques were employed in conducting NAPTC Test 165 and, hence, these errors are smaller than those present in the earlier NAPTC Tests 88 and 91 which were discussed in Ref. 5.

ever, is proceeding, and a complete evaluation for NAPTC Test 165 will be carried out and reported appropriately in the future. Finally, these two estimates (first branch and second branch) of these "externally-applied forces" each with an appropriate "reliability weighting factor" will be combined in a Kalman-filter subprogram of TEJ-JET to provide an "optimum estimate" of the transient impact/interaction forces experienced by each mass point station of the ring.

Based upon the studies already conducted including the use of the first branch of the TEJ-JET process, one may conclude that the adequacy and the accuracy of the experimental data as well as the effectiveness of the analytical techniques employed have improved to a point where plausible TEJ-JET estimates of the total impact/interaction forces can be deduced. Similar success is anticipated with respect to the second force-estimate branch of TEJ-JET.

In addition to the transient deformed-ring position data provided photographically, it is believed that measurements of transient strains on the ring could be employed as an additional element in TEJ-JET to obtain further improvements in the estimated transient externally-applied forces. Accordingly, for TEJ-JET as well as for checking CIVM-JET predictions (Refs. 7 and 10), increased attention to obtaining accurate transient strain measurements is recommended. Finally, it should be noted that the basic idea behind the TEJ-JET process is such that, in principle, if proved to be practically feasible, it can be applied to deduce the transient external forces applied to containment/deflector rings under arbitrary kinds of fragment attack: (a) single blade attack, (b) n-fragment attack, (c) impact from one or more blades from a fully bladed rotor, etc. Hence, a final evaluation of the practical feasibility of this method is anticipated anxiously.

REFERENCES

1 Chiarito, P.T., "Status of Engine Rotor Burst Protection Program for Aircraft." NASA Aircraft Safety and Operating Problems Conference, Langley Research Center, May 4-6, 1971. NASA SP-270. (N71-30756.)

2 Anon., "Disk Plating Cited in 747 Engine Incident", Aviation Week and Space Technology, February 28, 1972, pp. 50-51.

3 DeLucia, R.A., and Mangano, G.J., "Rotor Burst Protection Program: Statistics on Aircraft Gas Turbine Engine Failures that Occurred in Commercial Aviation During 1971." NAPTC-PE-12, February 1973. (Available as NASA CR-121151.)

4 McCallum, R.B., Leech, J.W., and Witmer, E.A., "Progress in the Analysis of Jet Engine Burst-Rotor Containment Devices." Massachusetts Institute of Technology, Aeroelastic and Structures Research Laboratory, ASRL TR 154-1, August 1969. (Available as NASA CR-107900.)

5 McCallum, R.B., Leech, J.W., and Witmer, E.A., "On the Interaction Forces and Responses of Structural Rings Subjected to Fragment Impact." Massachusetts Institute of Technology, Aeroelastic and Structures Research Laboratory, ASRL TR 154-2, September 1970. (Available as NASA CR-72801.)

6 Leech, J.W., Witmer, E.A., and Yeghiayan, R.P., "Dimensional Analysis Considerations in the Engine Rotor Fragment Containment/Deflection Problem." Massachusetts Institute of Technology, Aeroelastic and Structures Research Laboratory, ASRL TR 154-3, December 1971. (Available as NASA CR-120841.)

7 Wu, R. W-H., and Witmer, E.A., "Finite-Element Analysis of Large Transient Elastic-Plastic Deformations of Simple Structures, with Application to the Engine Rotor Fragment

Containment/Deflection Problem." Massachusetts Institute of Technology, Aeroelastic and Structures Research Laboratory, ASRL TR 154-4, January 1972. (Available as NASA CR-120886.

8 Zirin, R.M., and Witmer, E.A., "Examination of the Collision Force Method for Analyzing the Responses of Simple Containment/Deflection Structures to Impact by One Engine Rotor Blade Fragment." Massachusetts Institute of Technology, Aeroelastic and Structures Research Laboratory, ASRL TR 154-6, May 1972. (Available as NASA CR-120952).

9 Wu, R. W-H., and Witmer, E.A., "Computer Program - JET 3 - to Calculate the Large Elastic-Plastic Dynamically-Induced Deformations of Free and Restrained, Partial and/or Complete Structural Rings." Massachusetts Institute of Technology, Aeroelastic and Structures Research Laboratory, ASRL TR 154-7, August 1972. (Available as NASA CR-120993).

10 Collins, T.P. and Witmer, E.A., "Application of the Collision-Imparted Velocity Method for Analyzing the Responses of Containment and Deflector Structures to Engine Rotor Fragment Impact", Massachusetts Institute of Technology, Aeroelastic and Structures Research Laboratory, ASRL TR 154-8, August 1973. (Available as NASA CR-134494.)

11 Martino, A.A., and Mangano, G.J., "Turbine Disk Burst Protection Study. Phase I -- Final Report on Problem Assignment NASA DPR R-105." NAEC-AEL-1793 U.S. Navy, March 1965. (Available as NASA CR-80962.)

12 Martino, A.A., and Mangano, G.J., "Turbine Disk Burst Protection Study. Phases II and III -- Final Report on Problem Assignment NASA DPR R-105." NAEC-AEL-1848, U. S. Navy, February 1967. (Available as NASA CR-84967.)

13 Martino, A.A., and Mangano, G.J., "Rotor Burst Protection Program Initial Test Results. Phase IV -- Final Report on Problem Assignment NASA DPR R-105." NAPTC-AED-1869, U.S. Navy, April 1968. (Available as NASA CR-95967.)

14 Martino, A.A., and Mangano, G.J., "Rotor Burst Protection Program. Phase V -- Final Report on Problem Assignment NASA DPR R-105." NAPTC-AED-1901, May 1969. (Available as NASA CR-106801.)

15 Mangano, G.J., "Rotor Burst Protection Program, Phases VI and VII -- Exploratory Experimentation to Provide Data for the Design of Rotor Burst Fragment Containment Rings." NAPTC-AED-1968, March 1972. (Available as NASA CR-120962.)

16 Osborne, E.E., "Smallest Least Squares Solutions of Linear Equations", J. SIAM Series B: Numerical Analysis, Vol. 2, p. 300 (1965).

17 Kellogg, W.C., private communication, Massachusetts Institute of Technology, Lincoln Laboratory, 1972-73.

18 Hildebrand, F.B., Introduction to Numerical Analysis, McGraw-Hill Book Co., New York, 1956.

19. Private communication from F.B. Hildebrand, 1972.

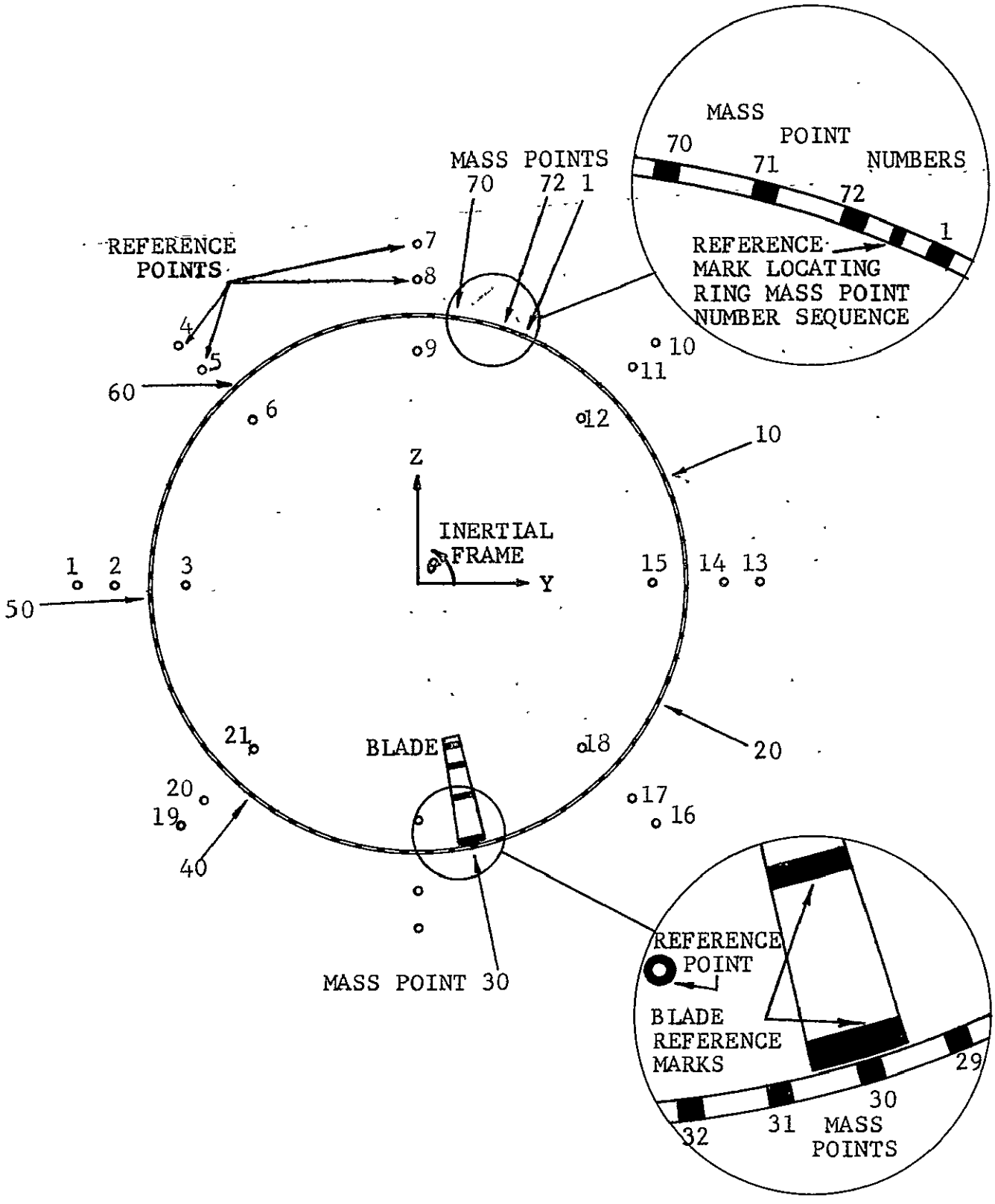

FIG. 1 SINGLE-BLADE CONTAINMENT TEST SET-UP FOR NAPTC TEST 165
IDENTIFYING DATA STATIONS IN THE PRE-IMPACT CONDITION

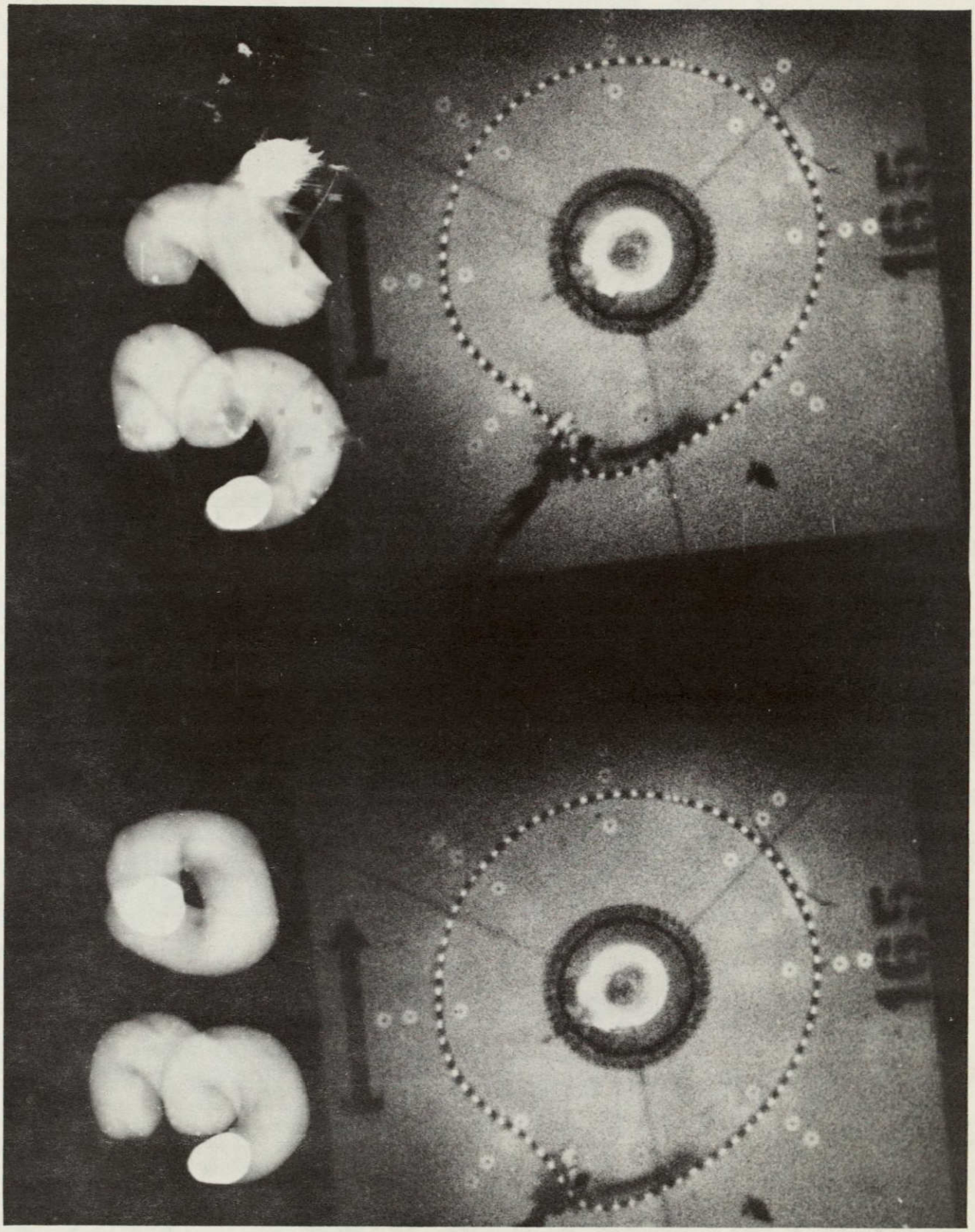

FIG. 2 SAMPLE OF HIGH-SPEED PHOTOGRAPHIC RECORD FROM NAPTC TEST 165 SHOWING POST-IMPACT CONDITIONS AT t = 900 AND 960 MICROSECONDS

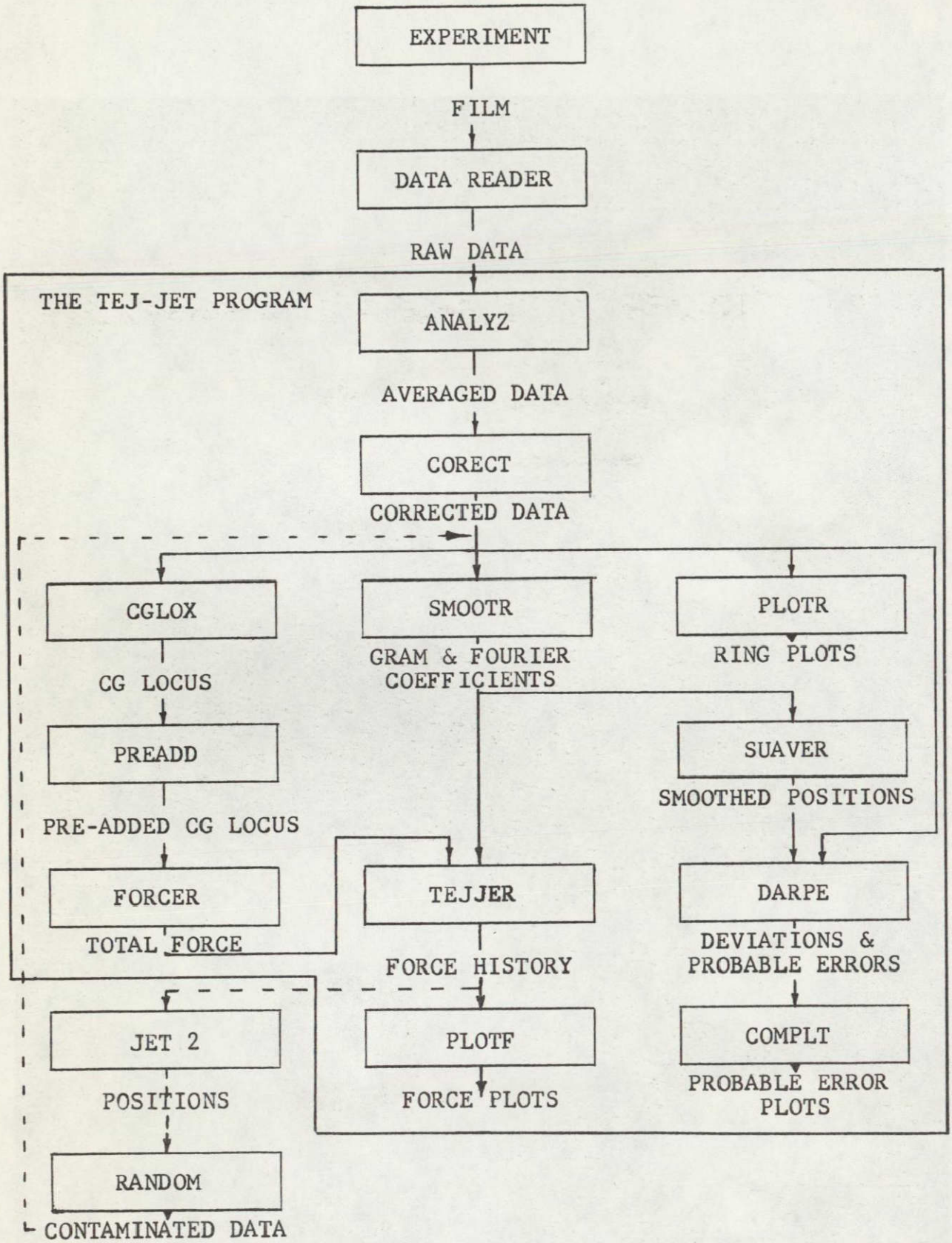

FIG. 3 ROTOR BURST CONTAINMENT DATA REDUCTION SCHEMATIC FOR THE TEJ-JET PROGRAM

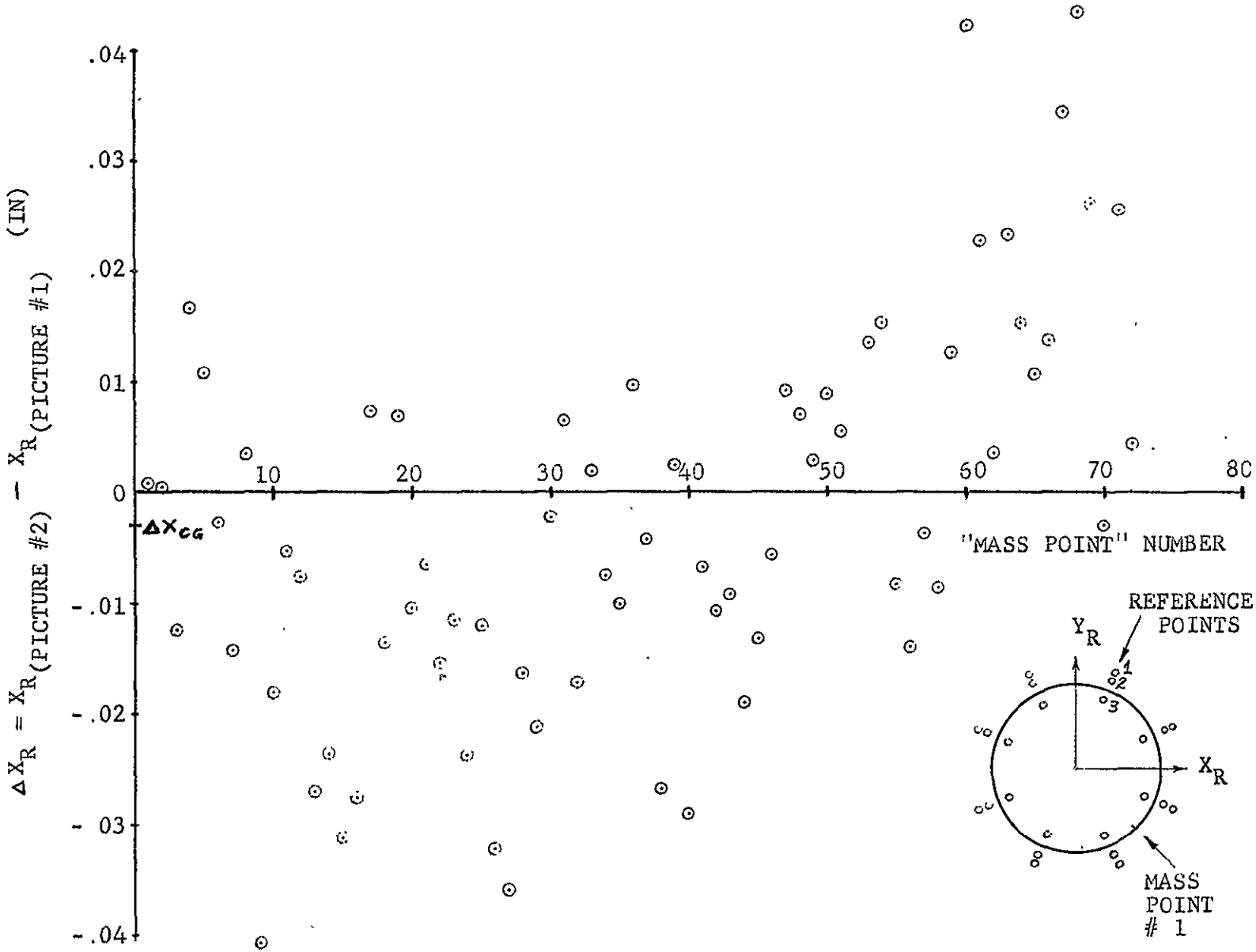

(a) Horizontal Component

FIG. 4 VARIATIONS IN CONTAINMENT RING "MASS POINT" POSITIONS AS OBTAINED FROM PRE-IMPACT PICTURES ONE AND TWO

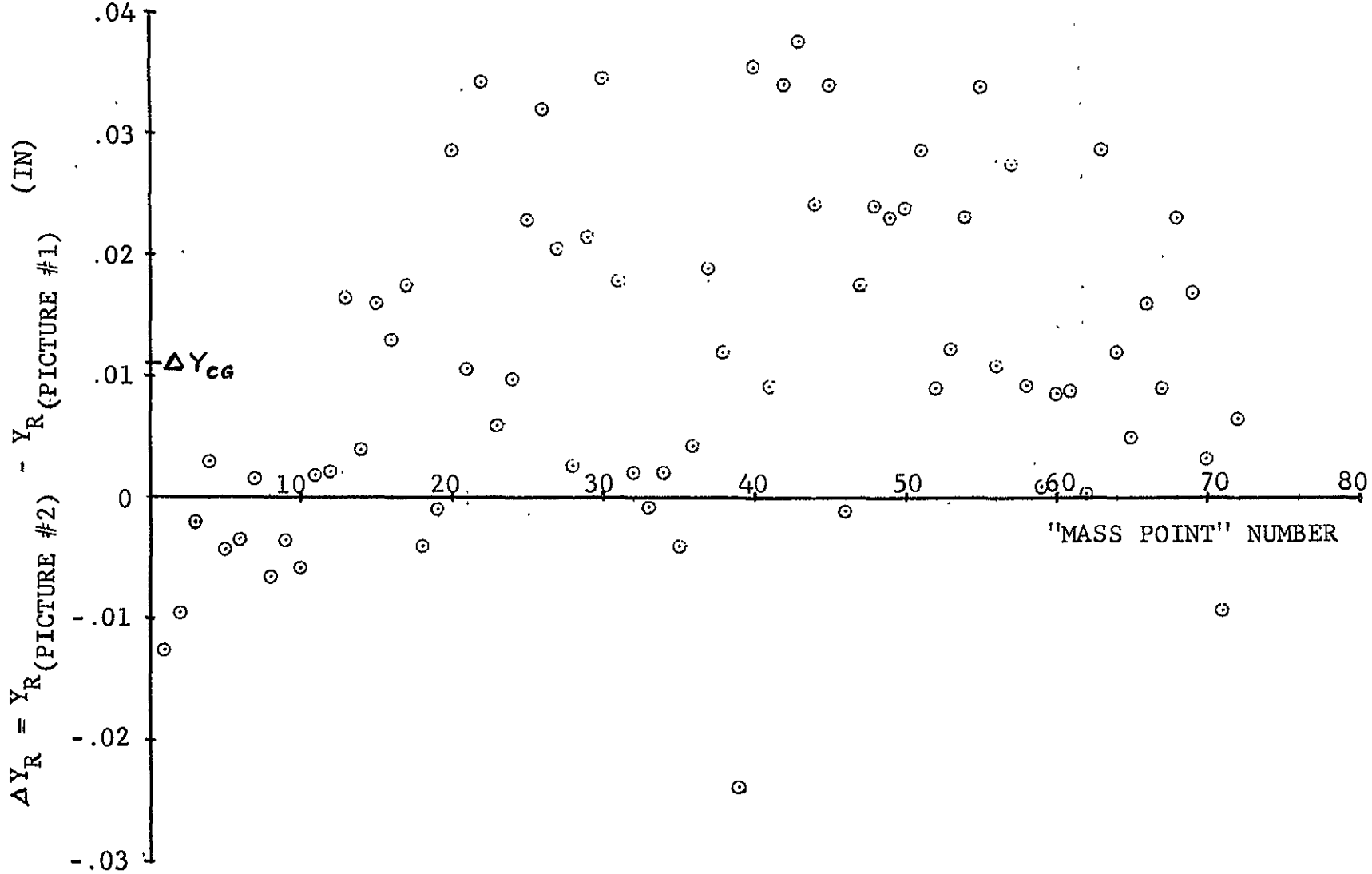

(b) Vertical Component

FIG. 4 CONCLUDED

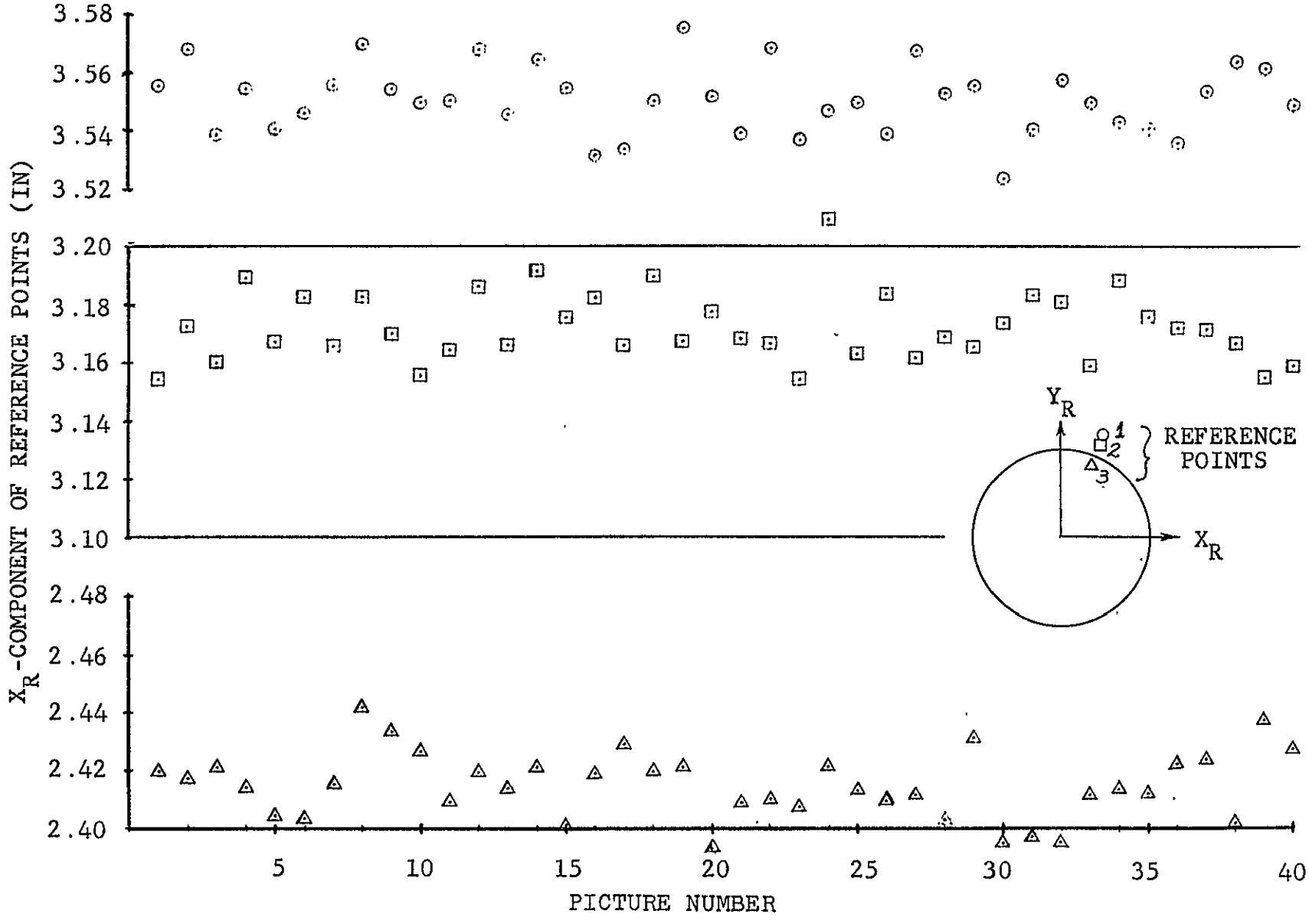

(a) Horizontal Component

FIG. 5 SAMPLE OF DATA SCATTER IN STATIONARY BACKGROUND REFERENCE POINT POSITION TIME HISTORY

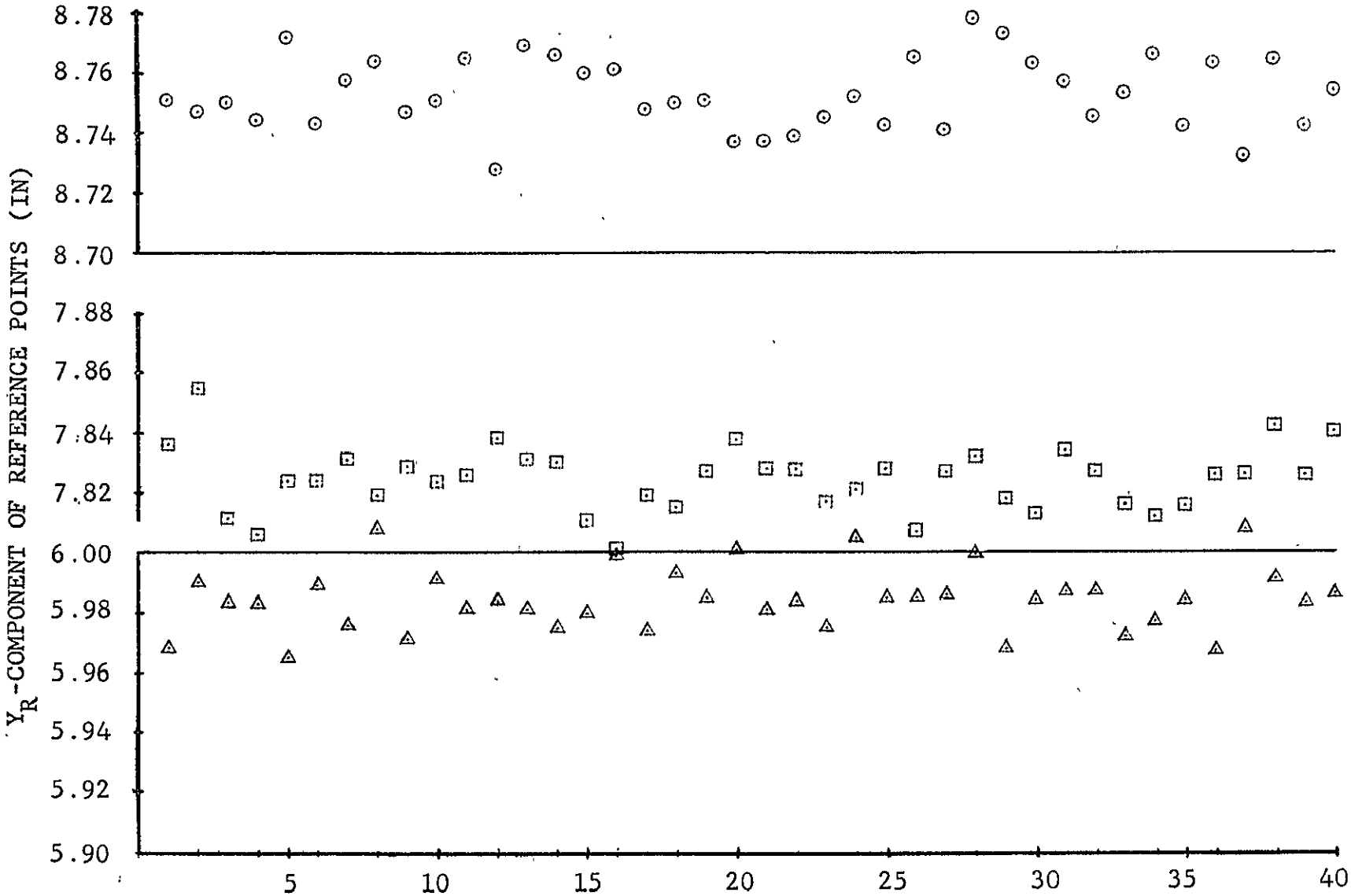

(b) Vertical Component

FIG. 5 CONCLUDED

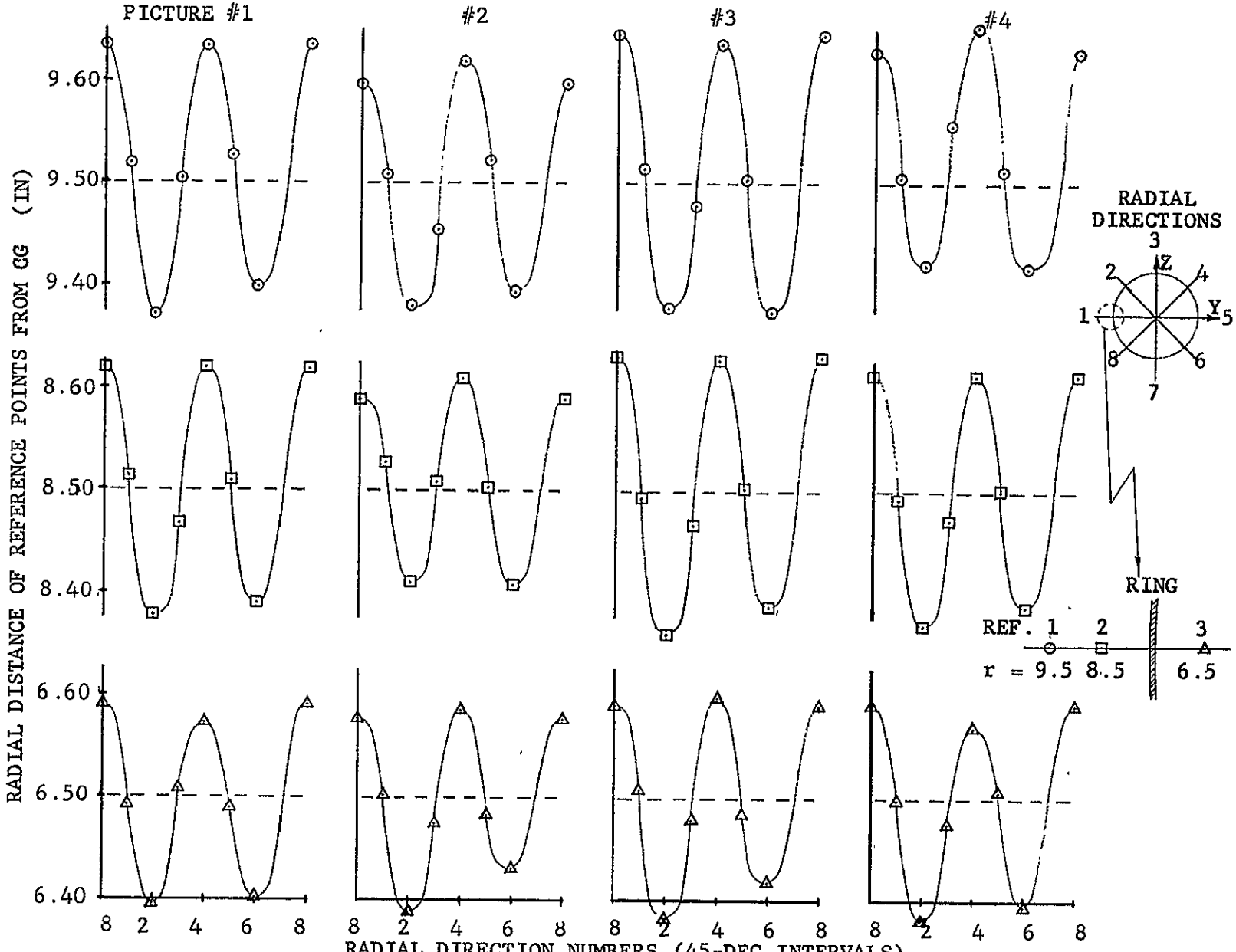

(a) Radial Component

FIG. 6 SAMPLE OF OPTICAL DISTORTION IN IMAGE OF REFERENCE POINTS

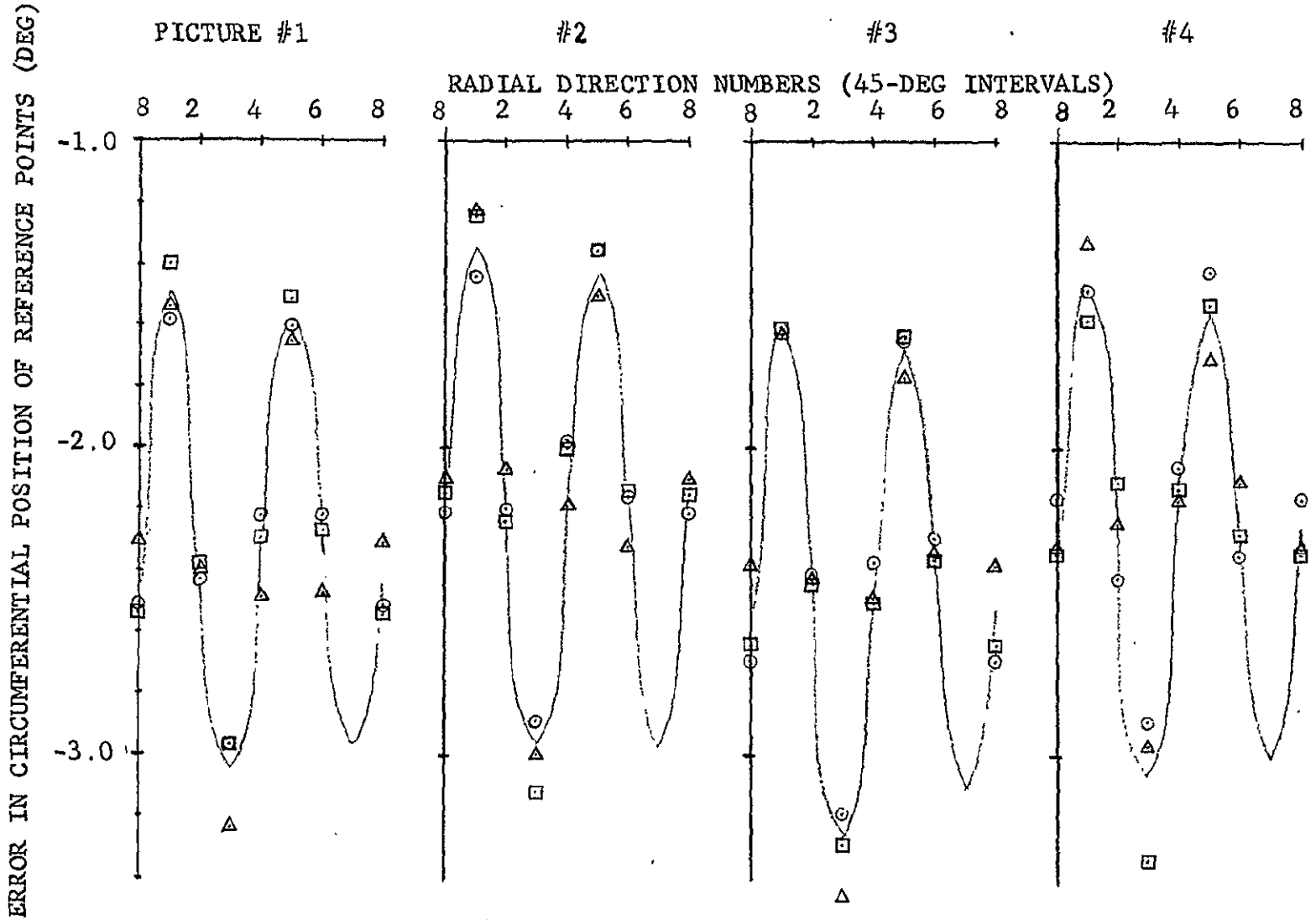

(b) Circumferential Component

FIG. 6 *CONCLUDED*

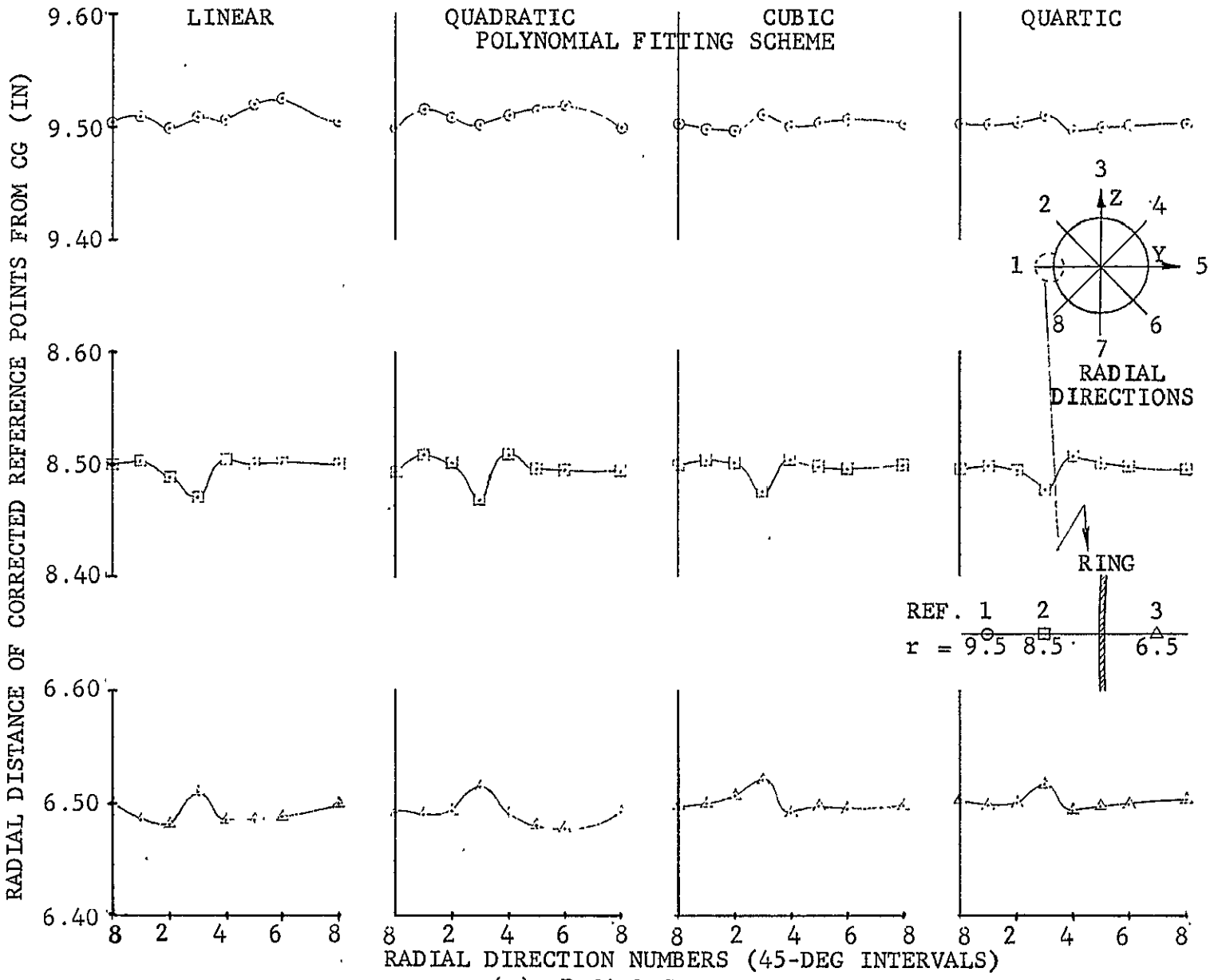

(a) Radial Component

FIG. 7 SAMPLE OF REFERENCE POINT POSITION DATA AS CORRECTED BY POLYNOMIAL FITTING SCHEME

(b) Circumferential Component

FIG. 7 CONCLUDED

LINEAR, QUADRATIC, OR CUBIC POLYNOMIAL FITTING SCHEME

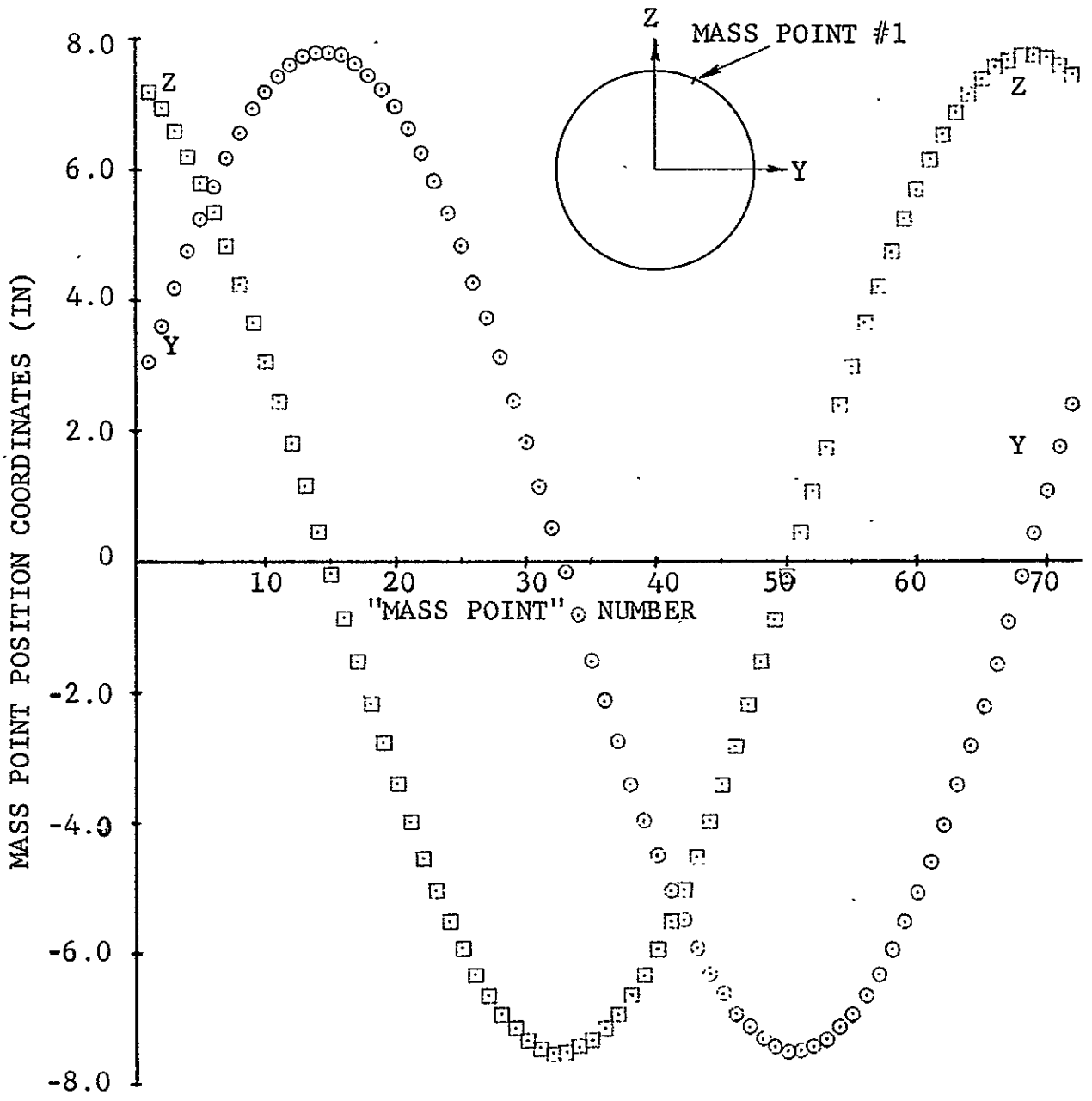

FIG. 8 CONTAINMENT RING PRE-IMPACT "MASS POINT" POSITION DATA FROM PICTURE ONE AS CORRECTED BY POLYNOMIAL FITTING SCHEME

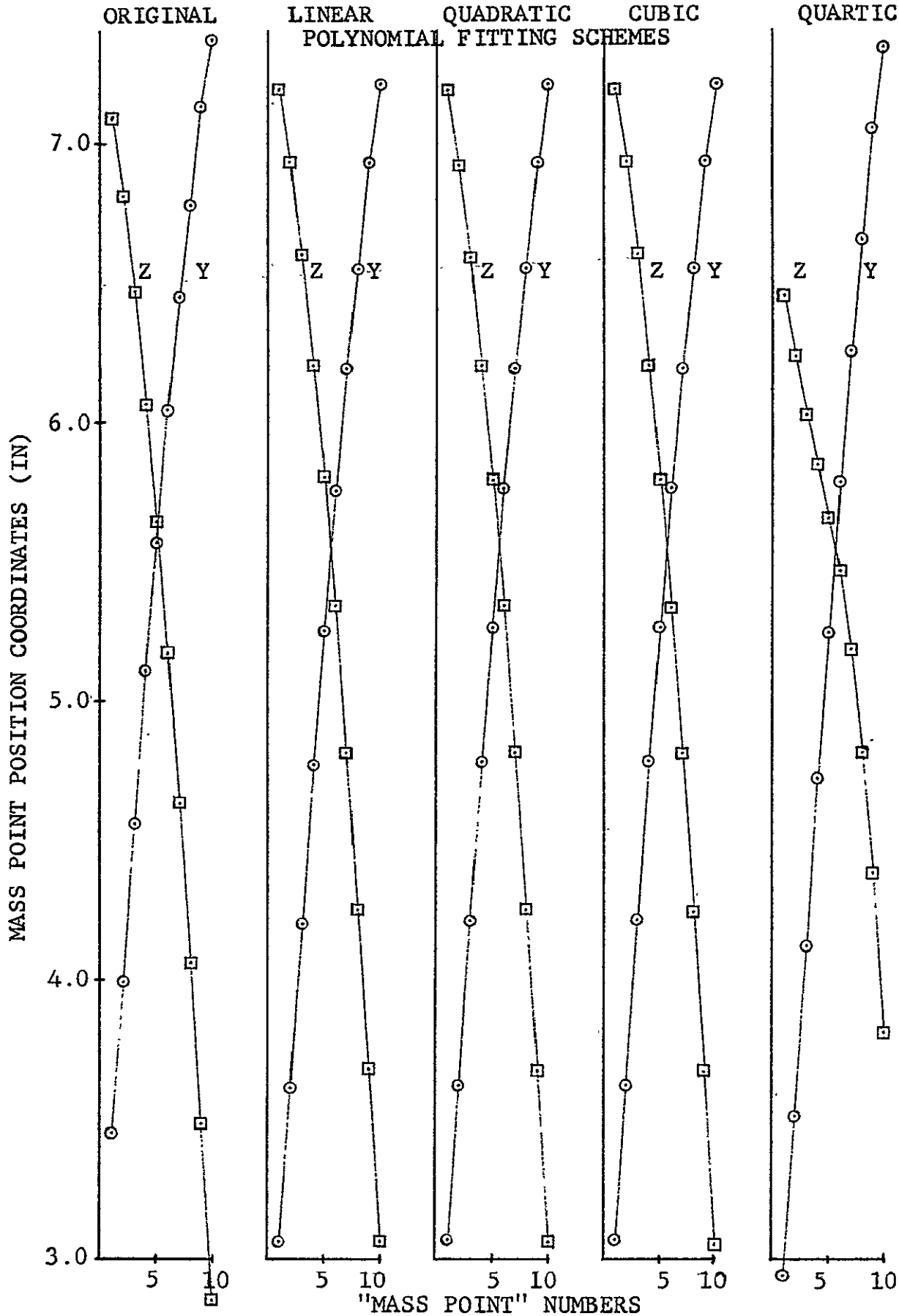

FIG. 9 DETAIL OF CORRECTED PRE-IMPACT POSITION DATA FOR A SEGMENT OF THE RING SHOWING EFFECT OF ORDER OF POLYNOMIALS EMPLOYED IN FITTING SCHEME

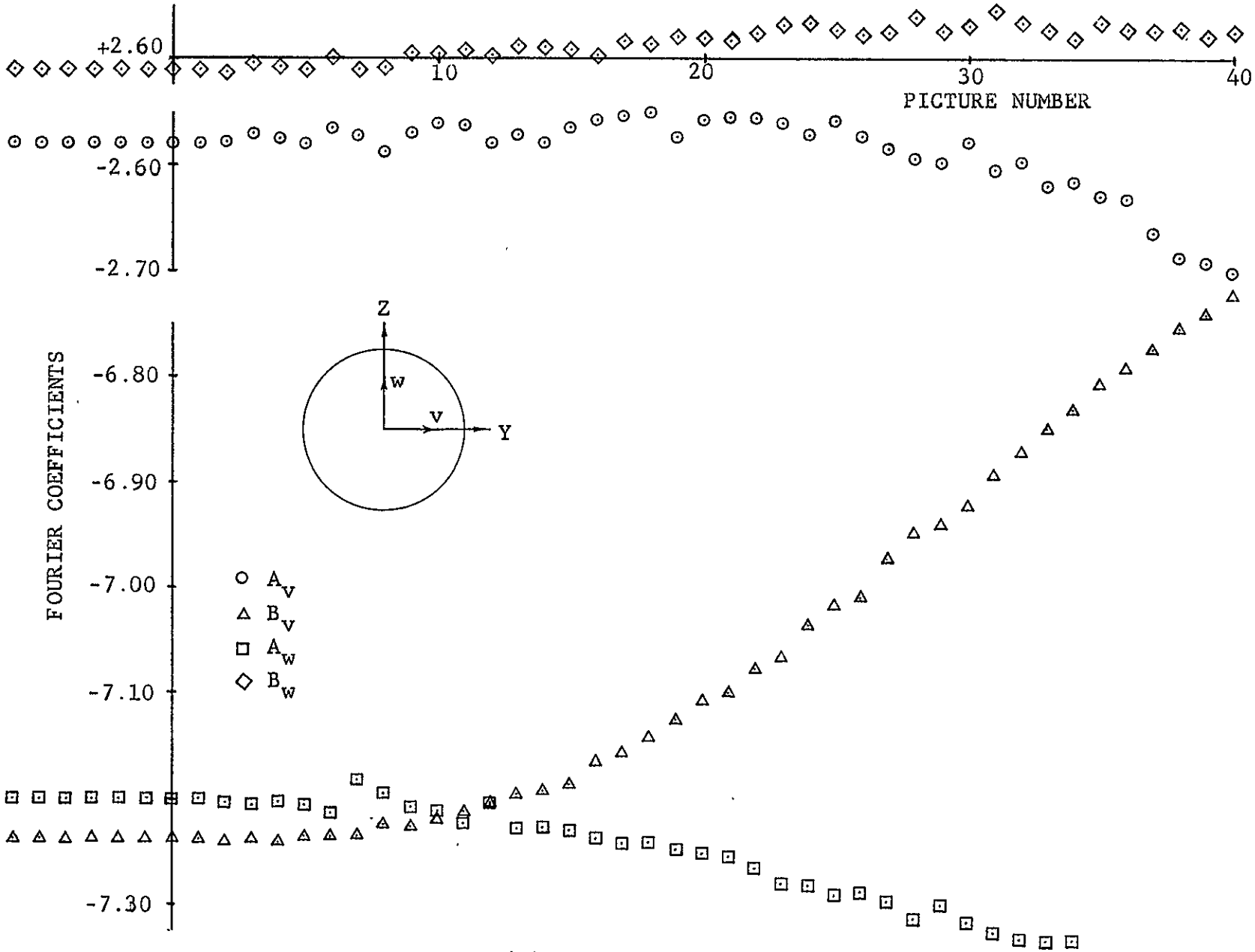

(a) First Fourier Harmonic

FIG. 10 TIME HISTORY OF FOURIER COEFFICIENTS USED FOR SPATIAL SMOOTHING OF RING "MASS POINT" POSITION DATA

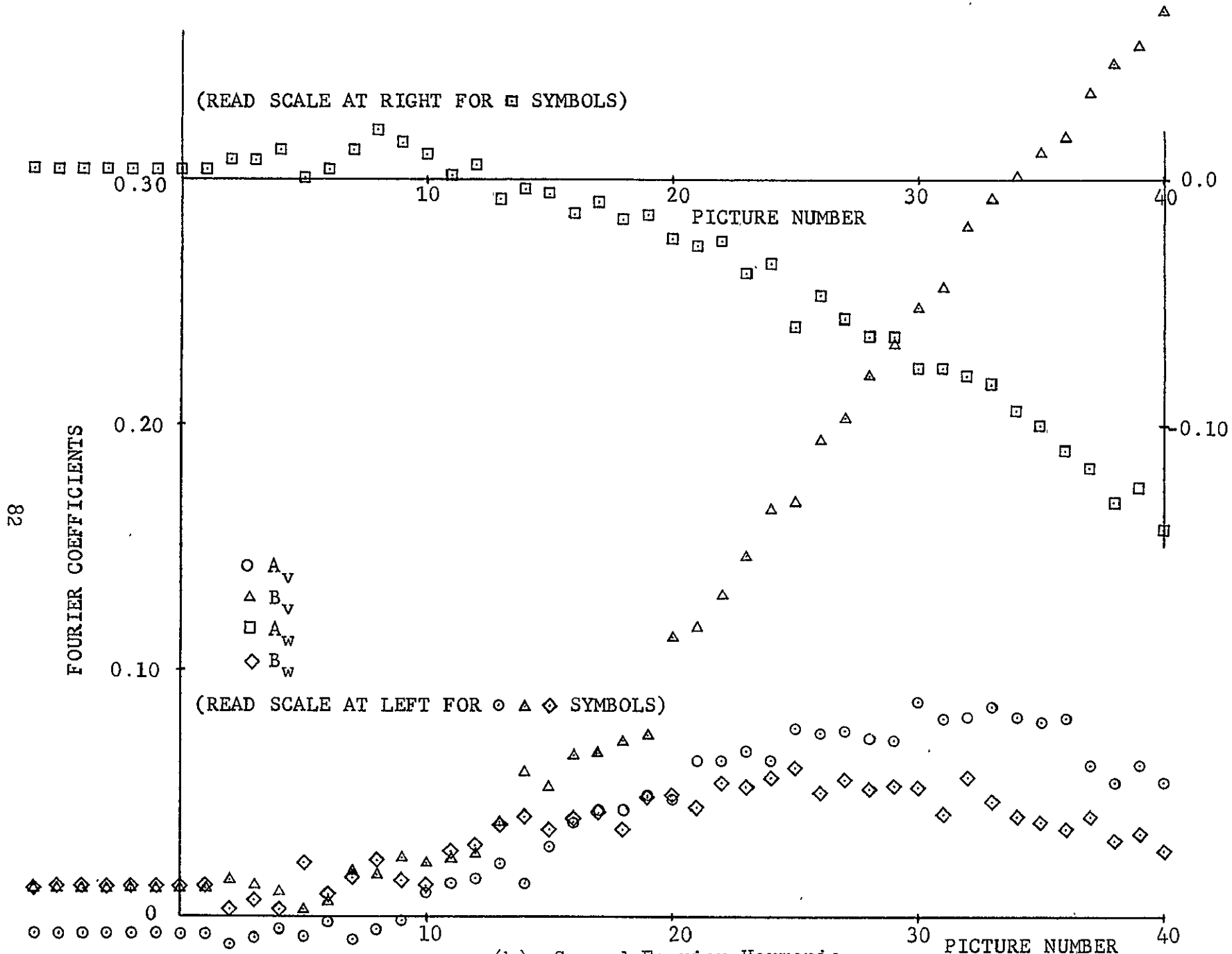

(b) Second Fourier Harmonic

FIG. 10 CONTINUED

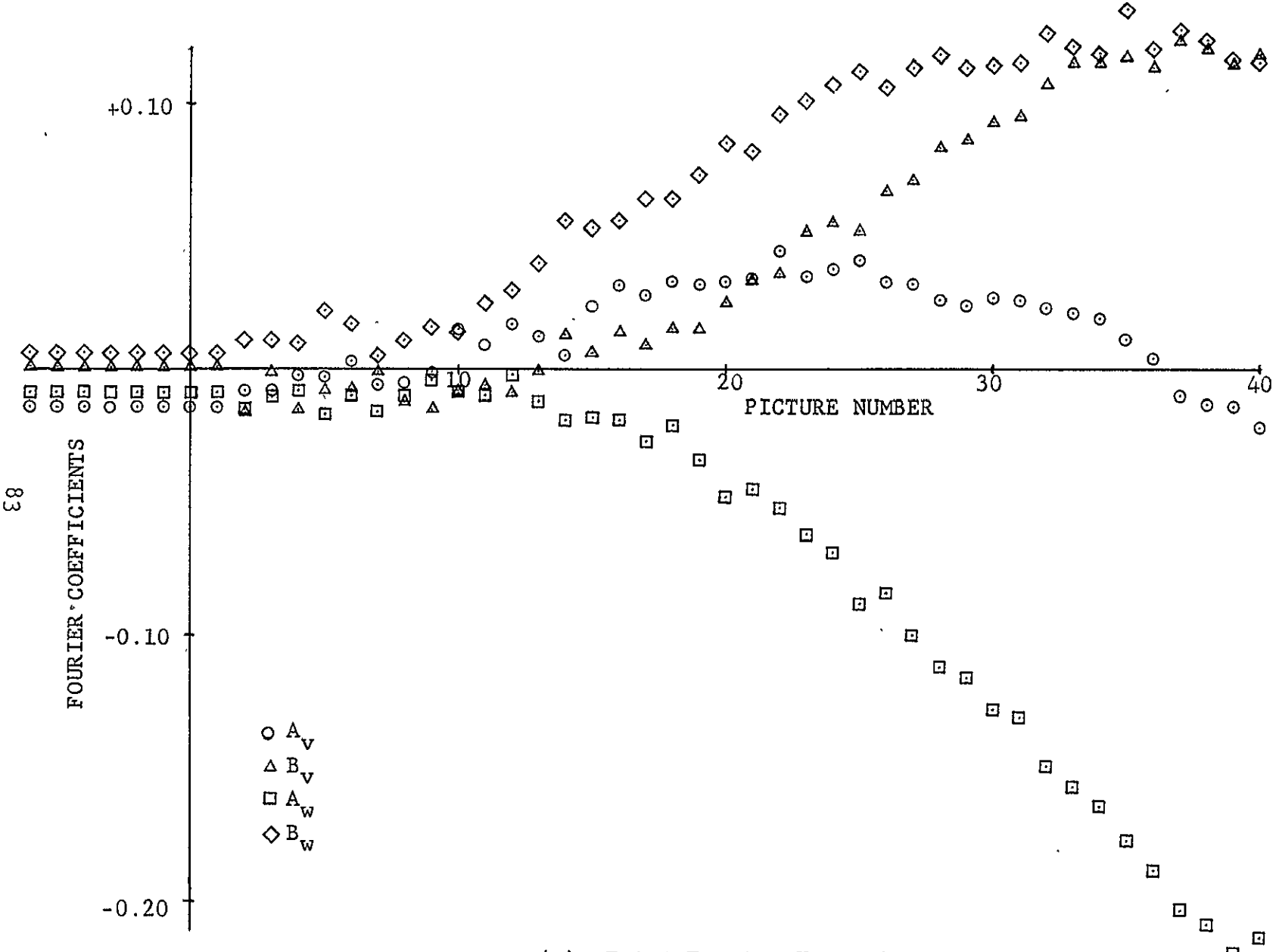

(c) Third Fourier Harmonic

FIG. 10 CONCLUDED

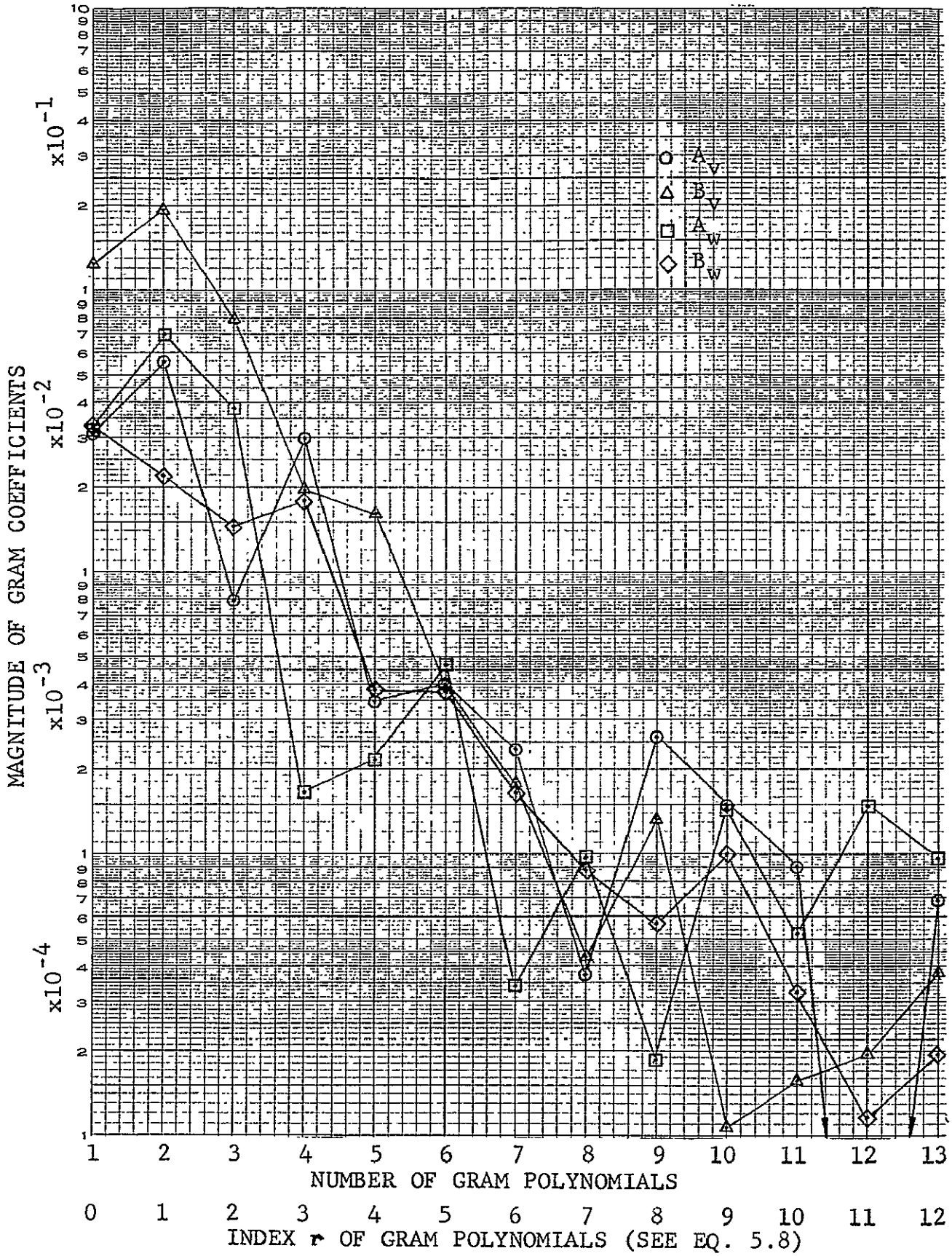

FIG. 11 MAGNITUDES OF GRAM COEFFICIENTS USED FOR TIMEWISE SMOOTHING OF COEFFICIENTS OF SECOND FOURIER HARMONIC

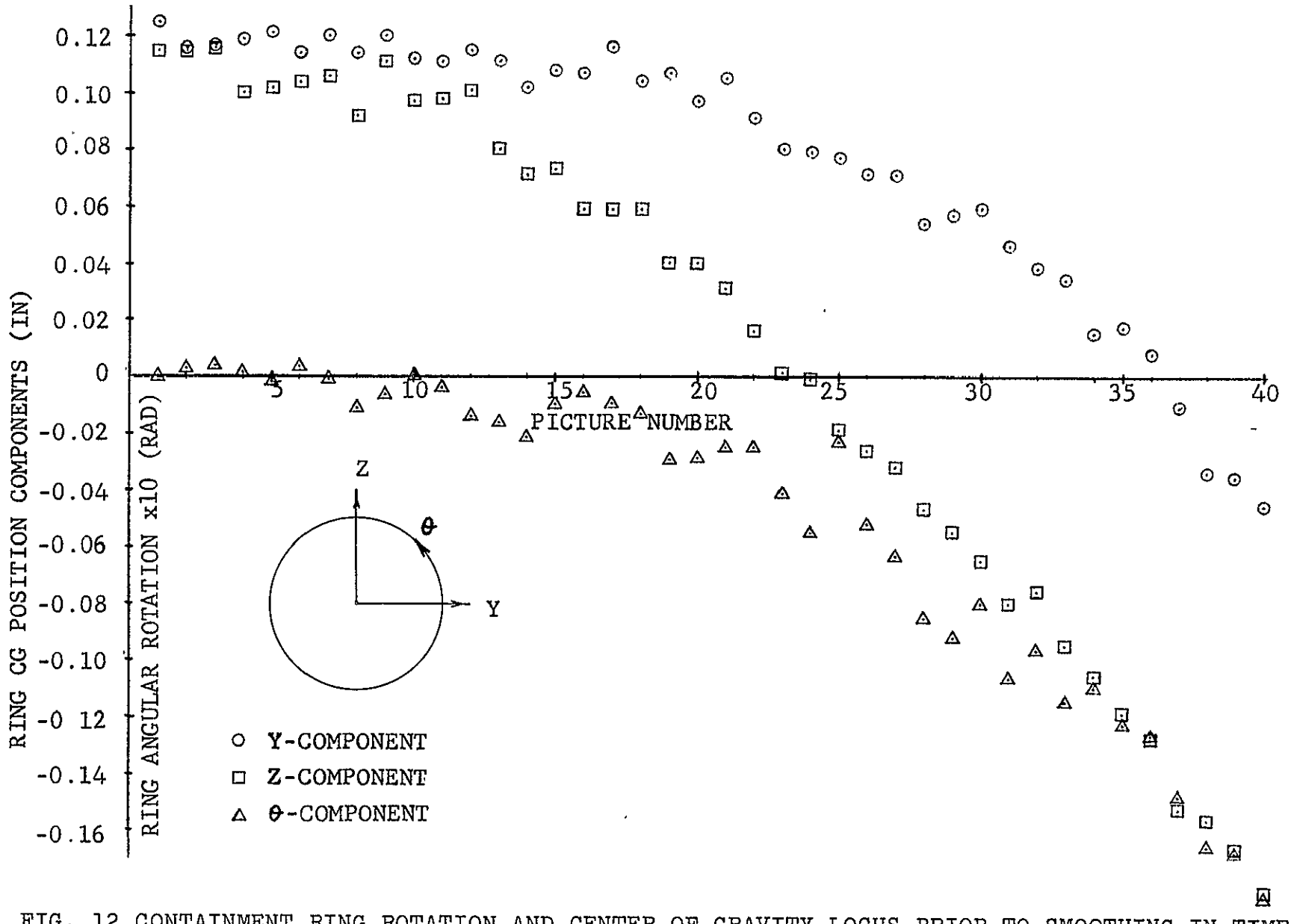

FIG. 12 CONTAINMENT RING ROTATION AND CENTER-OF-GRAVITY LOCUS PRIOR TO SMOOTHING IN TIME

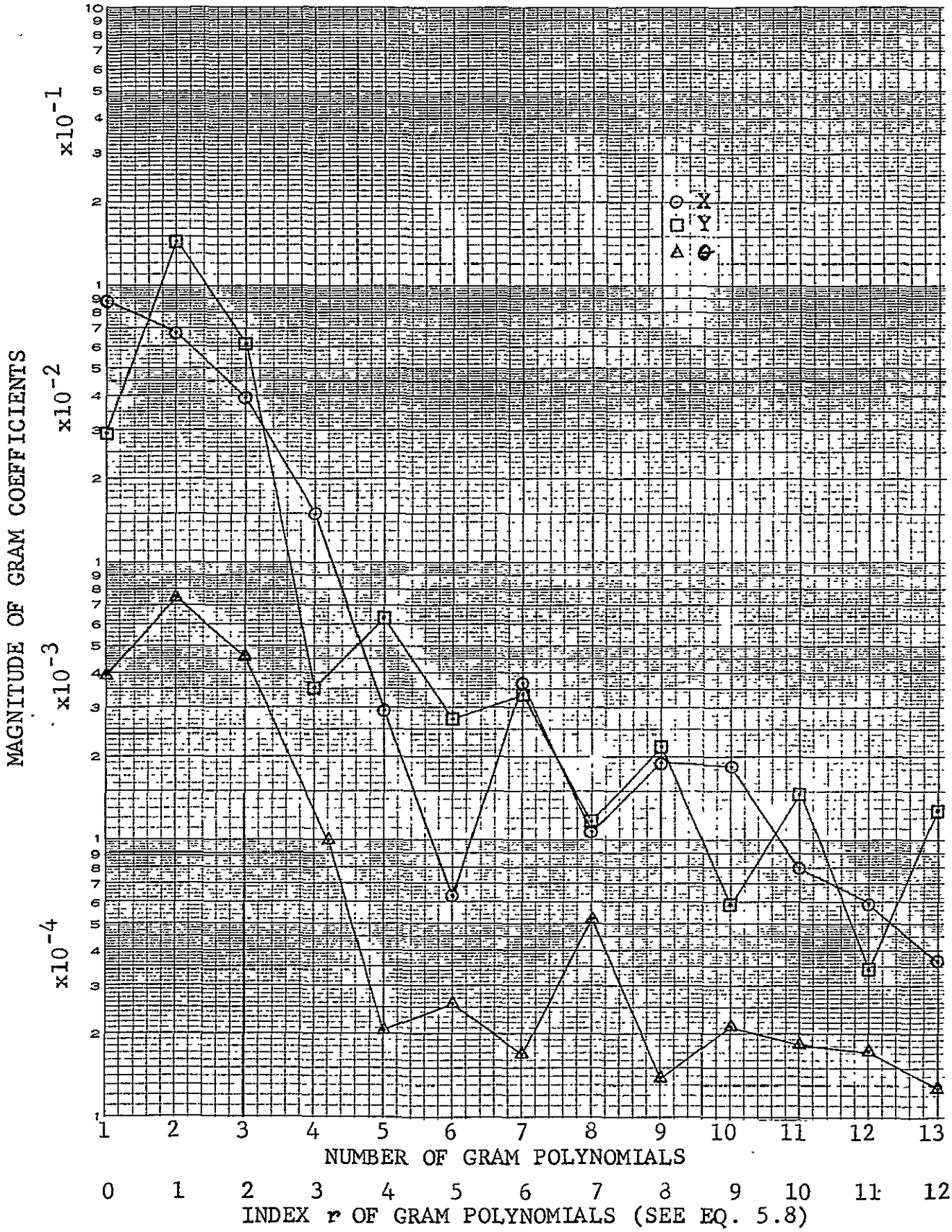

FIG. 13 MAGNITUDES OF GRAM COEFFICIENTS USED FOR TIMEWISE SMOOTHING OF RING CG LOCUS AND ANGULAR ROTATION

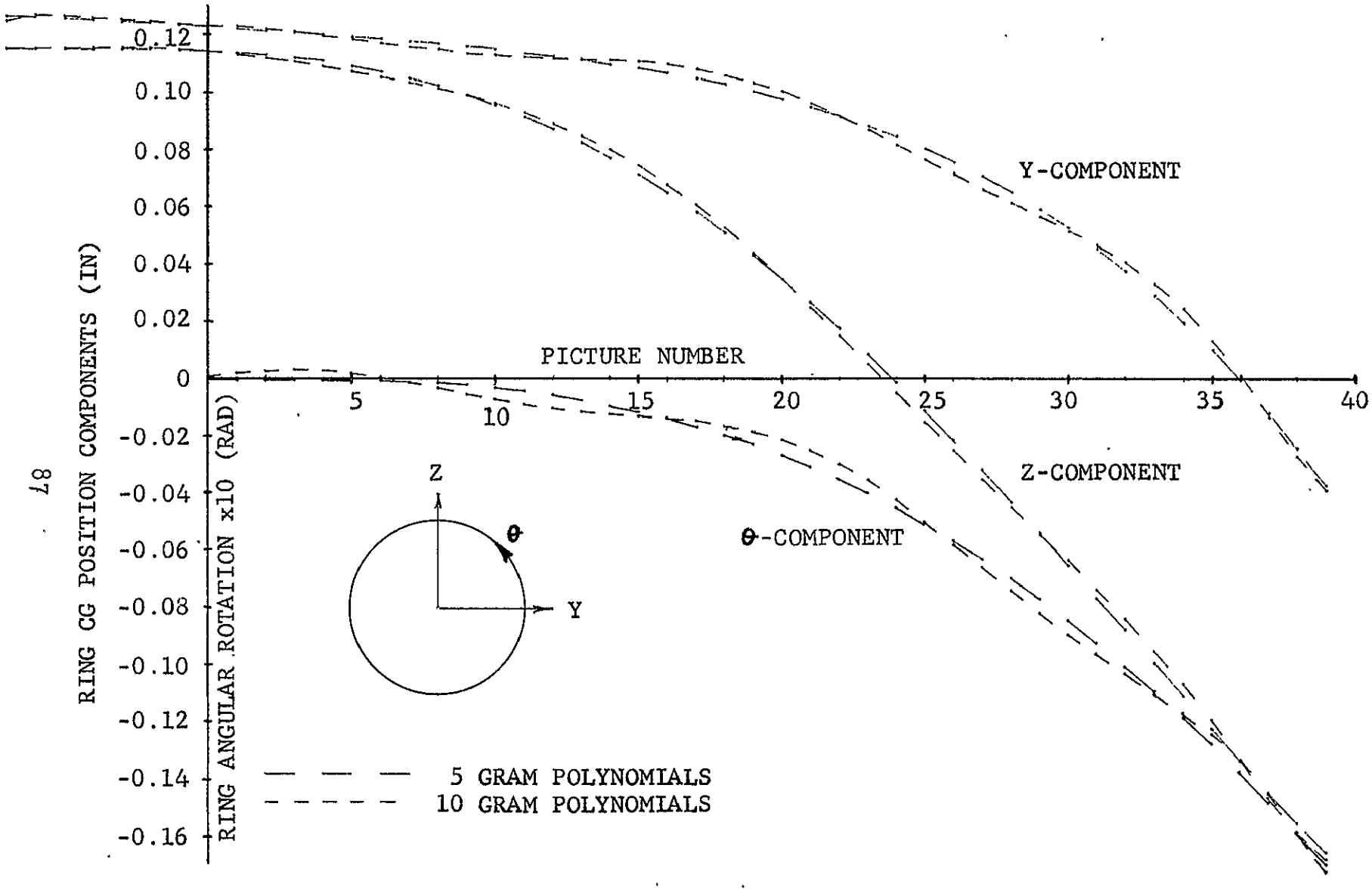

FIG. 14 SAMPLE OF RING ROTATION AND CG LOCUS AS SMOOTHED IN TIME BY GRAM POLYNOMIALS

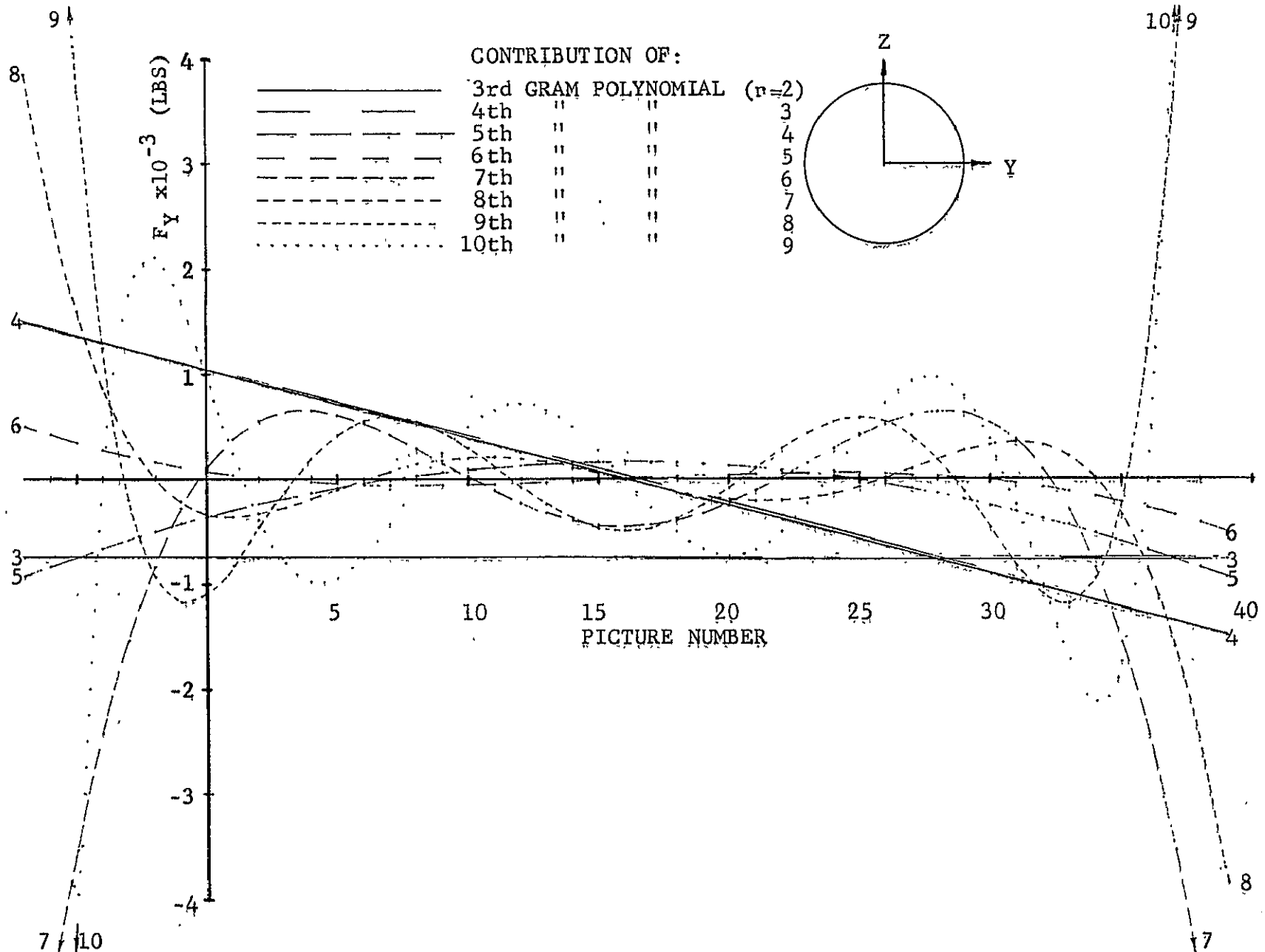

FIG. 15 CONTRIBUTIONS OF INDIVIDUAL GRAM POLYNOMIALS TO CG-ESTIMATED TOTAL FORCE ACTING ON RING

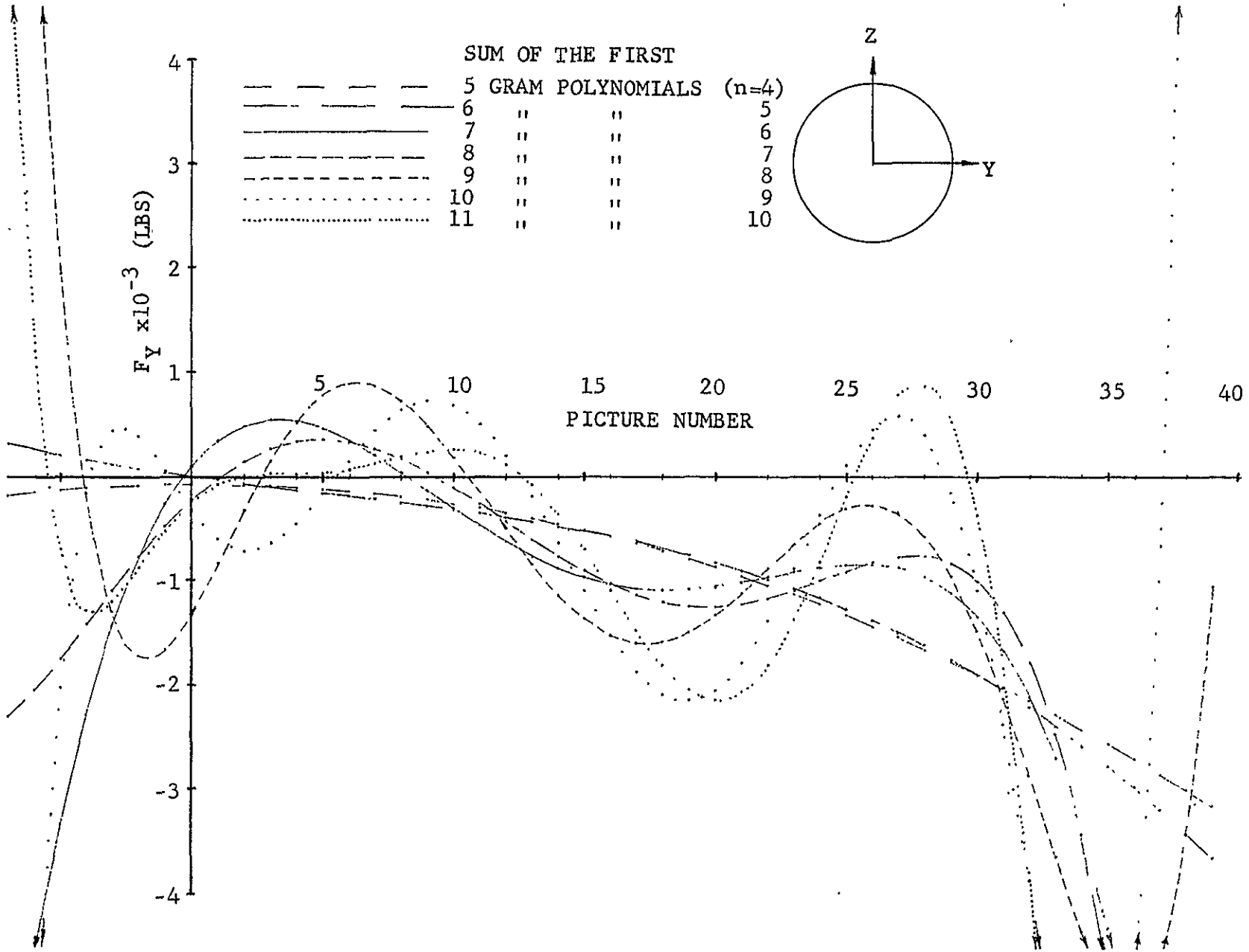

(a) Horizontal Component

FIG. 16 ESTIMATED TOTAL FORCE ACTING ON RING AS A FUNCTION OF NUMBER OF GRAM POLYNOMIALS USED FOR TIMEWISE SMOOTHING OF CG LOCUS

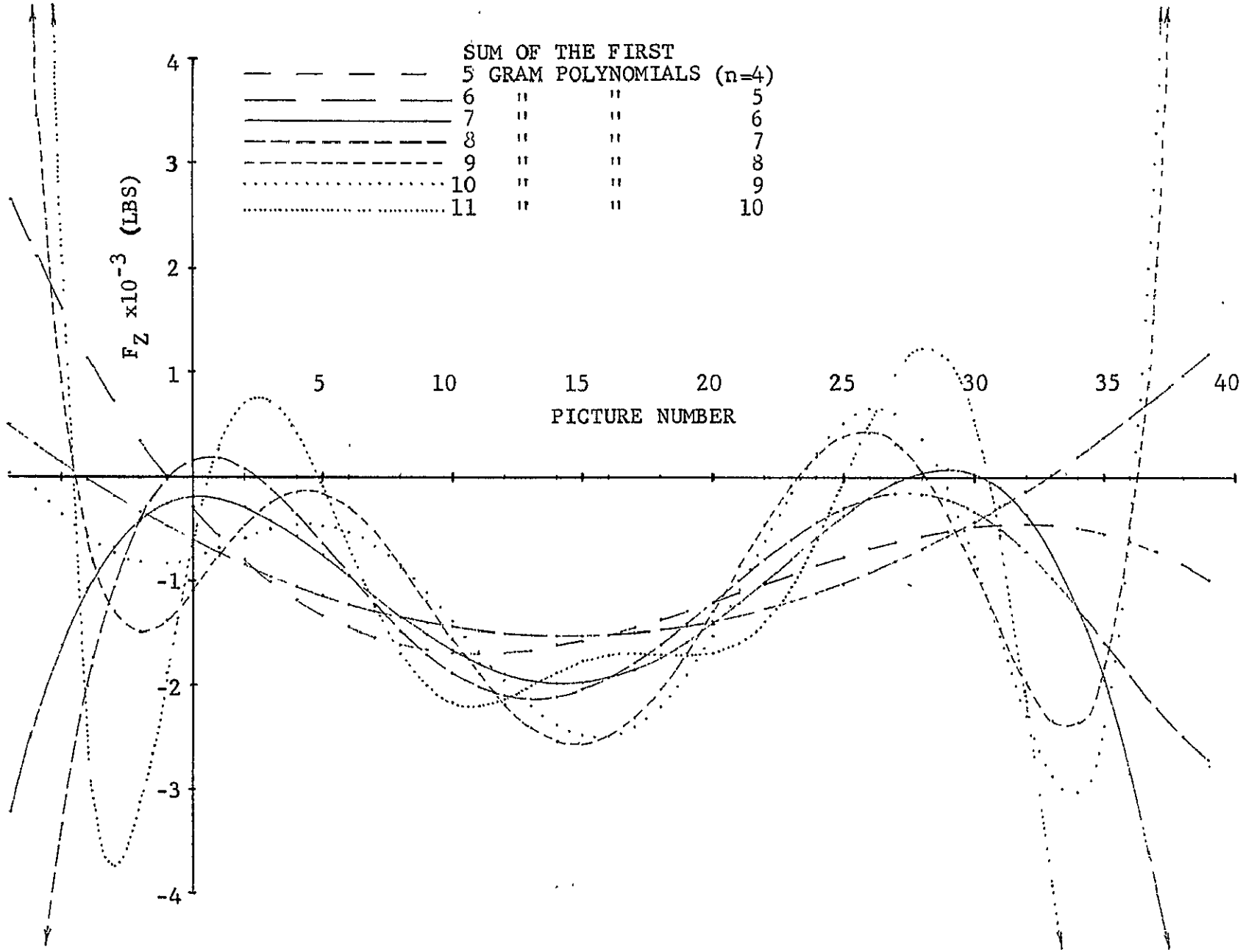

(b) Vertical Component
FIG. 16 CONCLUDED

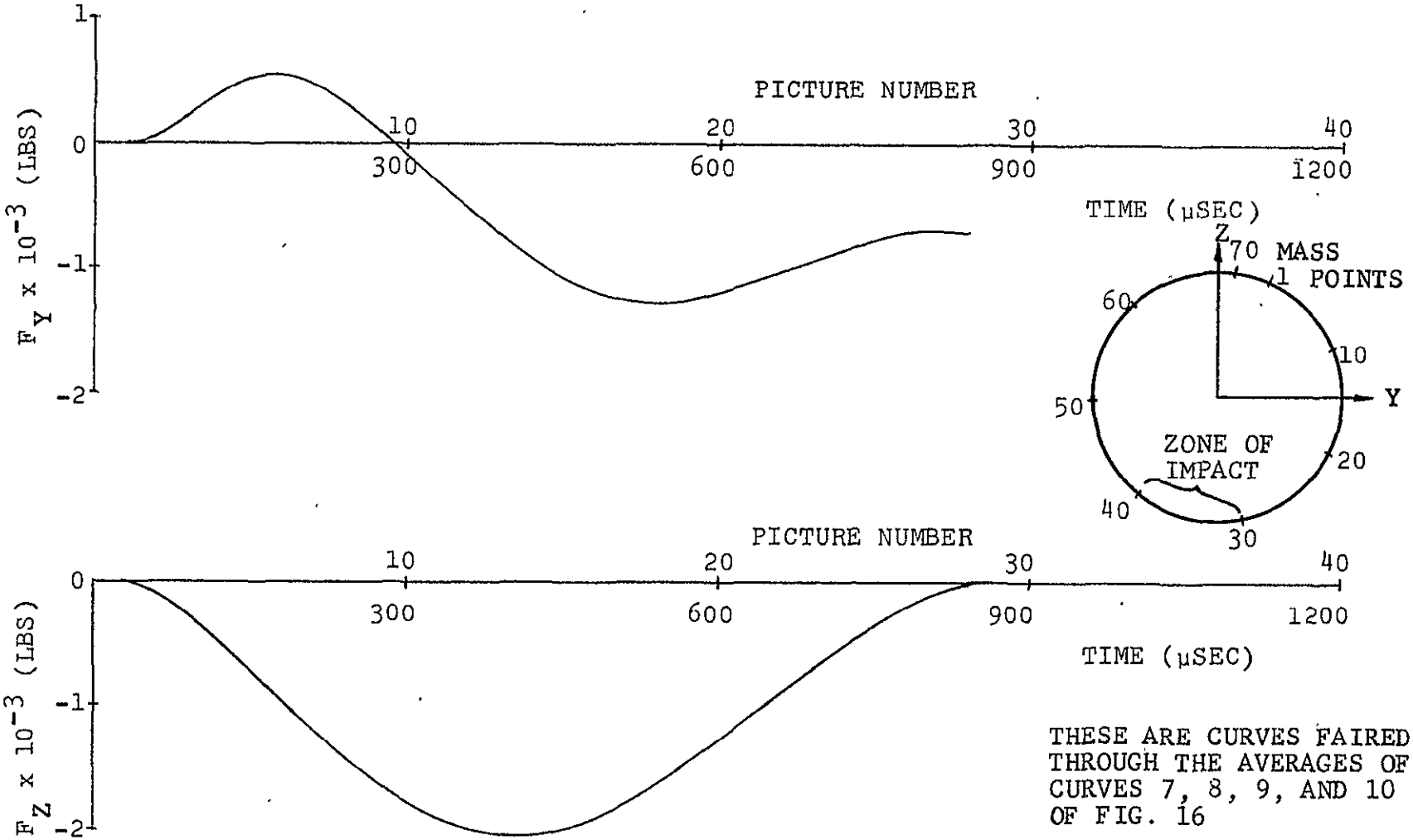

FIG. 17 TIME HISTORY OF COMPONENTS OF ESTIMATED TOTAL COLLISION-INDUCED FORCE ACTING ON RING

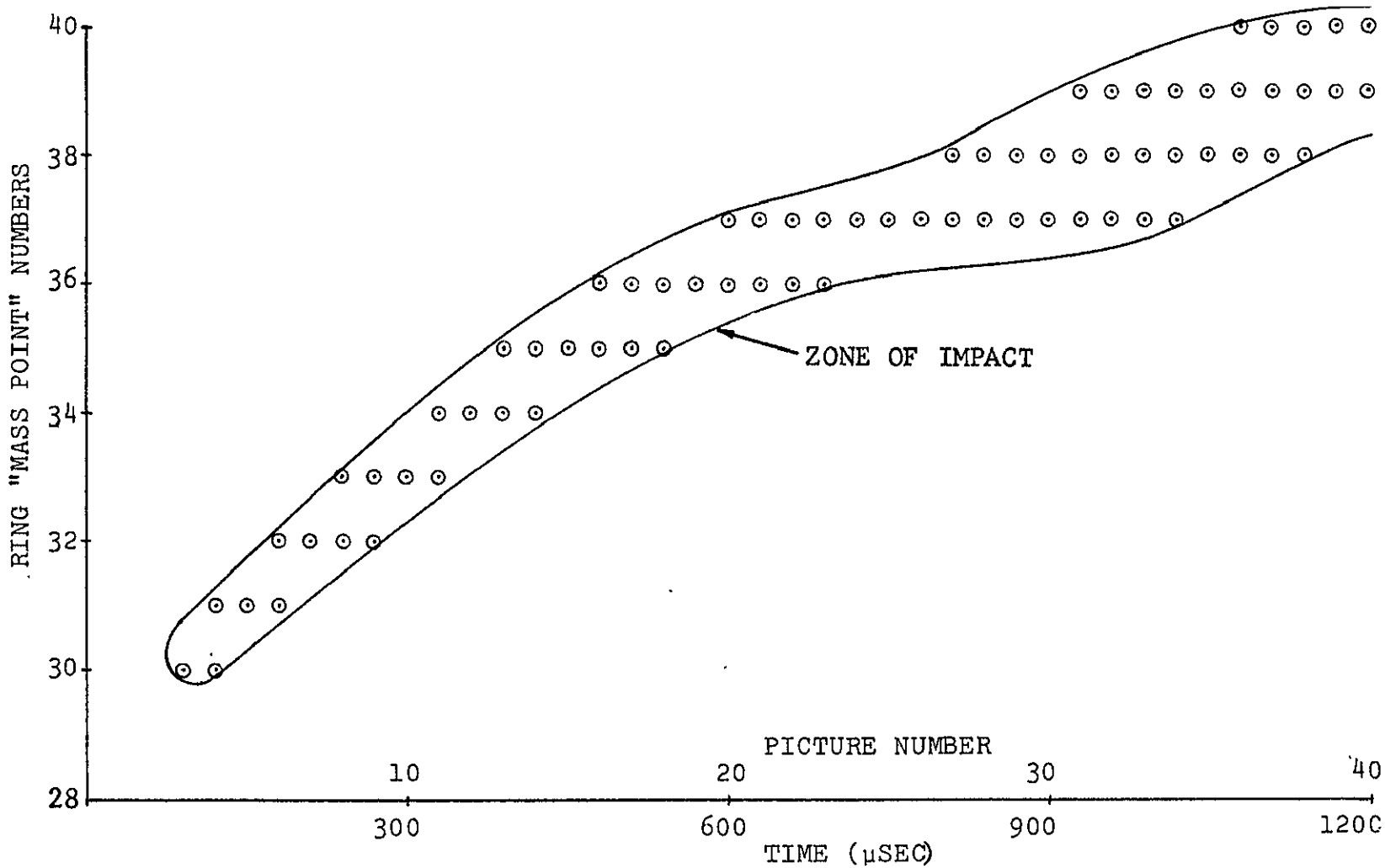

FIG. 18 TIME HISTORY OF ZONE OF BLADE IMPACT ON RING "MASS POINT" STATIONS

THE FOLLOWING PAGES ARE DUPLICATES OF ILLUSTRATIONS APPEARING ELSEWHERE IN THIS REPORT. THEY HAVE BEEN REPRODUCED HERE BY A DIFFERENT METHOD TO PROVIDE BETTER DETAIL